Article

Screening of Ionic Liquids and Deep Eutectic Solvents for Physical CO₂ Absorption by Soft-SAFT Using Key Performance Indicators

Ismail I. I. Alkhatib, Margarida L. Ferreira, Carlos G. Alba, Daniel Bahamon, Fèlix Llovell, Ana B. Pereiro, João M. M. Araújo, Mohammad R.M. Abu-Zahra, and Lourdes F. Vega*

Cite This: *J. Chem. Eng. Data* 2020, 65, 5844−5861

Read Online

ACCESS | Metrics & More | Article Recommendations | Supporting Information

ABSTRACT: The efficient screening of solvents for CO₂ capture requires a reliable and robust equation of state to characterize and compare their thermophysical behavior for the desired application. In this work, the potentiality of 14 ionic liquids (ILs) and 7 deep eutectic solvents (DESs) for CO₂ capture was examined using soft-SAFT as a modeling tool for the screening of these solvents based on key process indicators, namely, cyclic working capacity, enthalpy of desorption, and CO₂ diffusion coefficient. Once the models were assessed versus experimental data, soft-SAFT was used as a predictive tool to calculate the thermophysical properties needed for evaluating their performance. Results demonstrate that under the same operating conditions, ILs have a far superior performance than DESs primarily in terms of amount of CO₂ captured, being at least two-folds more than that captured using DESs. The screening tool revealed that among all the examined solvents and conditions, $[C_4 py][NTf_2]$ is the most promising solvent for physical CO₂ capture. The collection of the acquired results confirms the reliability of the soft-SAFT EoS as an attractive and valuable screening tool for CO₂ capture and process modeling.
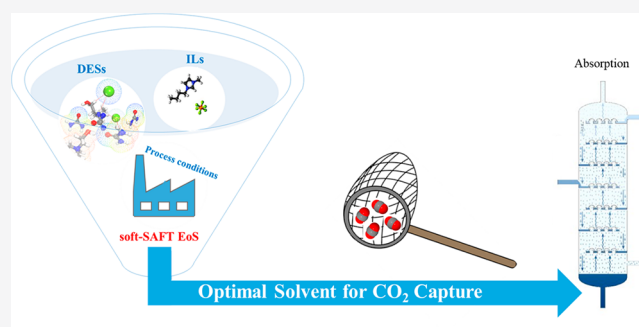
INTRODUCTION

Currently, the global energy market is substantially dependent on fossil fuels (i.e., coal, oil, and natural gas) as primary energy resources, with a dominating share of 84.3% through 2019.[1] The price paid for this behemoth dependency is the emergence of dire environmental issues manifested in global warming phenomenon and climate change, posing a threat to the sustenance of humanity on the planet in the long term. The primary precursor for these issues is the increasing global levels of carbon dioxide (CO₂) emissions, reaching 33.3 gigatons (Gt) by 2019, with almost 65% of these emissions generated solely from fossil fuel consumption either for power generation or industrial applications.[2]

Nowadays, carbon capture, utilization, and storage (CCUS) presents itself as the most feasible solution to this global issue in the near- and medium-terms.[3] The availability of an efficient and economically viable CO₂ capture technology is one of the cornerstones in the CCUS supply chain.[4] The absorption of CO₂ using aqueous solutions of alkanolamines, specifically monoethanolamine (MEA), is considered the industry golden standard, with the intrinsic advantage of being an "end-of-pipe" technology already implemented for purification and separation in other industrial applications.[5] Even though alkanolamines, with MEA as a benchmark, possess a high CO₂ absorption capacity, reactivity, and selectivity toward CO₂, their large-scale deployment for CO₂ capture is still marred

mainly by (1) the cost intensive solvent regeneration energy requirements, (2) degradability, either at the high temperature regeneration conditions or in the presence of oxygenated compounds commonly found in flue gases, (3) solvent losses due to high solvent volatility, and (4) high corrosivity jeopardizing the structural integrity of processing facilities.[4−6] These drawbacks are directly linked to their thermophysical properties such as high CO₂ absorption enthalpy, low thermal and chemical stability, high vapor pressure, and corrosive nature.[7]

Over the past decades, task-specific designed solvents such as ionic liquids (ILs), and deep eutectic solvents (DESs) have emerged as potential replacements to conventional aqueous amines for CO₂ capture. Both types of solvents belong to the low-transition-temperature mixtures family (LTTM), wherein a liquid substance is formed at low temperatures from a combination of individual components/species that otherwise would be solid at these conditions.[8,9] The prime advantage of these alternative solvents is their tunability feature, as their

synthesis is endowed with an additional degree of freedom due to the numerous combinations of possible starting materials.[9−11] The proper selection of the nature of individual components, and molar ratio in the case of DESs, allows a targeted synthesis of the solvent to specifically tailor unique thermophysical properties suited for a particular application. Among their many unique properties, the most attractive for CO_2 capture are their high chemical and thermal stability, and extremely low volatility, effectively limiting solvent losses and makeup.

A plethora of reviews exist in the literature compiling the extensive lab-scale experimental efforts toward the synthesis and application of ILs[6,7,9,12−16] and DESs[9,17−22] for CO_2 capture. Clearly, any technology newly developed for carbon capture should target improved performance to existing ones in technical, economic, and environmental aspects.[23,24] Nonetheless, the reported effectiveness of these solvents is often asserted with limited overall characteristics such as CO_2 solubility.[25] Additionally, some thermophysical properties of relevance for the design of CO_2 capture processes such as selectivity, enthalpy of absorption, heat capacity, diffusivity, viscosity, and surface tension are usually excluded from solvent performance evaluation. Thus, the conclusions drawn from these evaluations are misleading, as trade-offs between other important processing aspects affecting process design and operation such as heat of regeneration and mass transfer are overlooked.[26] The proper assessment of the potentiality of these solvents in a holistic manner would entail obtaining all relevant thermophysical properties at all industrially representative operations conditions.

Considering the wide array of synthesized ILs and DESs for CO_2 capture, experimentally acquiring all relevant information would be an unfeasible feat. Thus, it is imperative to develop a rapid and reliable screening procedure directly linking molecular characteristics of ILs and DESs to their overall carbon capture process performance. This can be accomplished through a reliable and appropriate thermodynamic model capable of reproducing the thermodynamic behavior of pure solvents and their mixtures with CO_2, integrated with rudimentary engineering calculations to assess the performance of these solvents in terms of key performance indicators (KPIs) such as solvent cyclic working capacity and energy of regeneration, among others. Robust screening tools of the sort have been successfully developed for the screening of various materials for CO_2 capture, such as conventional aqueous alkanolamines and their blends,[27,28] novel water-free hybrid solvents,[29,30] and adsorbents,[30−32] relying on sophisticated molecular modeling tools such as molecular-based equations of state (EoSs) and molecular simulation techniques to fully characterize the thermodynamic behavior of the CO_2 capture media.

In the case of screening tools developed for ILs and DESs for CO_2 capture, several contributions attempted such an endeavor,[25,33−52] with the limiting factor of their framework being the thermodynamic model of choice. These works relied on a variety of available models to obtain necessary thermodynamic information on these solvents, including conventional semiempirical correlations,[25,33,44,46−50] artificial intelligence (AI) techniques,[34,52,53] quantum chemistry calculations using the conductor like screening model for real solvents (COSMO-RS/SAC),[35−40,42,54] or a combination of these techniques.[43,45] Regression modeling approaches suffer from poor predictive accuracy outside the range of data used

for fitting, which can be enhanced with the utilization of an extensive amount of experimental data that might not be available. Moreover, they lack robustness as the full characterization of a single solvent would entail several models developed for each property of interest. Conversely, the COSMO-RS approach can be deemed predictive without need to adjust parameters to experimental data; however, in some cases the accuracy of the results is qualitatively compared to experimental data. The primary application for these models for solvent screening and evaluation has been limited to the confines of CO_2 solubility and enthalpy of absorption. However, these models have the potential to predict other thermophysical properties of importance for solvent screening (i.e., diffusivity, viscosity, surface tension, etc.) once integrated with other modeling approaches. For example, COSMO-RS have been used to obtain molecular descriptors for a wide variety of ILs, which integrated with machine learning algorithms, providing accurate predictions for viscosities of pure ILs.[55] The reader is referred to the comprehensive reviews of Vega et al.[10] and Alkhatib et al.[11] on the thermodynamic models applied in recent years on the characterization of ILs and DESs and criteria for model selection.

Alternatively, equations of state, particularly those based on the Statistical Associating Fluid Theory (SAFT),[56−59] provide a viable alternative for the development of solvent screening tools owing to their outstanding ability in capturing the physical nature of complex fluids in a representative manner. Additionally, these models are capable of predicting a full range of information needed for accurate process design and modeling, along with offering additional fundamental insight and understanding on the thermodynamic behavior of these solvents, encompassed in a single model. The strength of SAFT-based models stems from their strong theoretical framework deeply rooted in statistical mechanics based on the work of Wertheim's first-order thermodynamic perturbation theory (TPT1) of association.[60−63] This framework allows the explicit consideration of governing intermolecular interactions, such as dispersive, associating, polar, and others, expanding the range of fluids that can be modeled, being suitable to accurately describe the complex nature of ILs and DESs with the correct balance of accuracy, predictive power, and robustness.[10,11,64] Among the wide variety of SAFT-based EoSs, soft-SAFT by Blas and Vega[65,66] stands out for its robustness and accuracy in modeling the complex thermodynamic behavior of ILs[10,64,67−75] and DESs[11,76−78] and their wide range of applications. Moreover, soft-SAFT EoS has been successfully employed for the screening of a variety of solvents for CO_2 capture.[27−29,31]

In this contribution, we demonstrate the feasibility of employing a molecular-based EoS, the soft-SAFT EoS,[65,66] for the screening of physical solvents (i.e., ionic liquids and deep eutectic solvents) for CO_2 capture at industrially relevant conditions. This presents a key step toward the development of a suitable screening tool to identify the most promising solvents for CO_2 capture as well as for a more reliable process design simulation. The modeling tool is used to fully characterize the thermodynamic behavior of the pure solvents and their mixtures with CO_2 with a limited number of adjustable parameters. The soft-SAFT molecular models characterizing the thermodynamic behavior of pure ILs and DESs, and their mixtures with CO_2, are transferred from previous contributions, while those describing the viscosity of

pure solvents are developed in this work. These models are subsequently used in a predictive manner to describe key physical properties for CO_2 capture, integrated with simple engineering calculations to assess the potentiality of these solvents using KPIs such as cyclic working capacity, heat of regeneration, viscosity, diffusivity, and solvent consumption.

■ THEORY

The Soft-SAFT Equation of State (EoS). The general expression for the soft-SAFT EoS[65,66] computes the residual Helmholtz energy density (a^{res}) of a pure fluid by summing perturbation terms accounting for different structural and energetic contributions, as

$$a^{res} = a^{ref} + a^{chain} + a^{assoc} + a^{polar} \tag{1}$$

The reference term (a^{ref}) accounts for the contribution due to segment–segment repulsive and dispersive interactions for a Lennard-Jones (LJ) fluid in a single expression, computed from the LJ EoS of Johnson and co-workers.[79] The chain term (a^{chain}) represents the contribution arising from the formation of chains by connecting individual segments. The association term (a^{assoc}) exemplifies the contribution attributed to strong and highly directional short-range interactions such as those arising from the formation of hydrogen bonds. The expression for these two terms are obtained directly from Wertheim's TPT1,[60−63] being the same across all SAFT-based models. Lastly, in the case of polar interactions, an additional term is added (a^{polar}) to explicitly account for the contributions arising from polar forces such as dipolar and quadrupolar interactions. The expression for the polar term is based on the theory of Gubbins and Twu,[80,81] and its subsequent extension to chainlike fluids by Jog and Chapman.[82,83]

The thermodynamic modeling of fluids within the soft-SAFT framework entails acquiring a set of molecular parameters descriptive of major structural and energetic features of the fluid. The characterization of nonassociating fluids requires three parameters, namely, segment diameter (σ_i), chain length (m_i), and dispersive energy between segments (ε_i). In the case of associating fluids, two additional parameters are included, related to the volume (k^{HB}) and energy (ε^{HB}) of association. Lastly, explicitly modeling polar interactions requires the fraction of polar segments in the molecule (x_p) and the effective dipolar (D) or quadrupolar moment (Q). These molecular parameters are typically treated as adjustable parameters fitted using experimental saturated liquid density and vapor pressure of the pure fluid, while the dipolar and/or quadrupolar moment is taken from experimental information, and x_p is set *a priori* based on physical arguments.[84,85]

The extension of the model to multicomponent mixtures is straightforward for the chain, association, and polar terms, as they are explicitly written for mixtures. Alternatively, extending the reference term to multicomponent mixtures is done using the generalized Lorentz–Berthelot (LB) mixing rules, used to calculate the crossed diameter (η_{ij}) and energy (ε_{ij}):

$$\sigma_{ij} = \eta_{ij} \frac{(\sigma_{ii} + \sigma_{jj})}{2} \tag{2a}$$

$$\varepsilon_{ij} = \xi_{ij} \sqrt{\varepsilon_{ii}\varepsilon_{jj}} \tag{2b}$$

where η_{ij} and ξ_{ij} ($\eta_{ij} = 1 - l_{ij}$ and $\xi_{ij} = 1 - k_{ij}$ in classical EoSs) are the adjustable size and energy binary interaction parameters, respectively.

For mixtures of associating molecules, cross-association interactions between different molecules or different functional groups within the same molecules are computed using combining rules in a manner analogous to those in eqs 2a and 2b. The volume of cross-association is calculated by the mean arithmetic radius of the association site, while the energy of cross-association is calculated through the modified geometric average as follows:

$$\kappa_{ij}^{HB} = \left(\frac{\sqrt[3]{\kappa_{ii}^{HB}} + \sqrt[3]{\kappa_{jj}^{HB}}}{2} \right)^3 \tag{3a}$$

$$\varepsilon_{ij}^{HB} = \alpha_{ij}^{HB} \sqrt{\varepsilon_{ii}^{HB}\varepsilon_{jj}^{HB}} \tag{3b}$$

where α_{ij}^{HB} is a binary parameter that generalizes the energy of cross-association, fitted to binary mixture VLE data, if needed. The model is used in a fully predictive manner whenever the binary parameters (η_{ij}, ξ_{ij}, and α_{ij}^{HB}) are set to unity, without fitting to binary mixture vapor–liquid equilibrium (VLE) data.

Free-Volume Theory (FVT). Within the soft-SAFT framework, the viscosity of pure fluids is obtained using the free-volume theory (FVT),[86,87] wherein, the dynamic viscosity of a pure fluid (μ) is computed as the sum of two terms:

$$\mu = \mu_0 + \Delta\mu \tag{4}$$

where μ_0 is the viscosity of the dilute gas, which can be omitted for solvents with low vapor pressure due to its small contribution to the total viscosity,[88] and $\Delta\mu$ is the correction term used to account for the viscosity of the dense-state. By omitting the dilute gas term, the expression for the total viscosity becomes solely dependent on the dense-correction term which is computed based on the expression proposed by Allal and co-workers,[86,87] relating the microstructure and the free space among the molecules with the viscosity of the fluid using thermodynamic variables such as pressure, temperature, and density. The FVT dense term contains three adjustable parameters, α, B, and L_v, which are typically fitted to pure fluid or mixture viscosity data. Additional details on each FVT expression and their implementation within the framework of the soft-SAFT equation can be found in previous contributions.[89,90]

Extending viscosity calculations to multicomponent mixtures is done using linear compositional rules for each FVT adjustable parameter,[90] as such:

$$\alpha_{mix} = \sum_i x_i \alpha_i \tag{5a}$$

$$B_{mix} = \sum_i x_i B_i \tag{5b}$$

$$L_{v,mix} = \sum_i x_i L_{v,i} \tag{5c}$$

It should be noted that with these mixing rules, the model is extended to mixtures in a fully predictive manner, as no additional binary parameters are fitted to experimental viscosity data of the binary mixture. A detailed discussion will be provided in the results section.
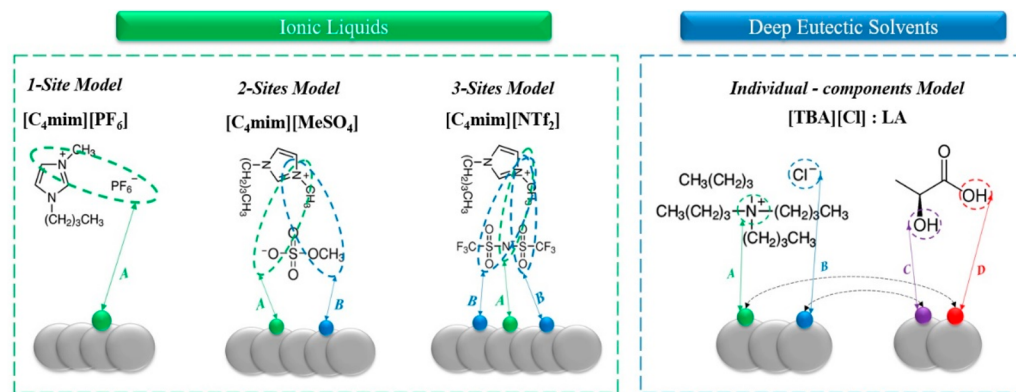
Figure 1. Representative examples of some ionic liquids and deep eutectic solvents examined in this work, and their counterpart soft-SAFT coarse-grain molecular models.

Key Performance Indicators for solvent screening. To properly evaluate the performance of ILs and DESs for CO_2 capture, the effectiveness of these solvents on three important elements with direct impact on the techno-economic feasibility of the absorption process is assessed. These elements are CO_2 solubility, mass transfer, and regeneration energy. For each element, a selection criterion is proposed based on fundamental engineering calculations, with the required input thermophysical properties directly predicted from soft-SAFT models developed for these solvents and their binary mixtures with CO_2. These selection criteria are subsequently used to capture the trade-offs in assessing the potentiality of these solvents in a comparative manner. As all the examined solvents present a physical absorption behavior for CO_2, their performance is assessed on the basis of a physical CO_2 absorption for precombustion CO_2 capture. In this process, the absorption of CO_2 from the feed flue gas takes place in an absorption column operated at low temperatures (298−313 K) and high pressures (1000−3000 kPa). The regeneration of the solvent occurs either by decreasing the operating pressure of the stripping column using a pressure swing absorption (PSA), or by increasing the temperature using a temperature swing absorption (TSA). For this work, it was opted to assess the performance of these solvents using a PSA process. It should be noted that the selectivity and effect of impurities on the performance of these solvents, though important for a final decision on the solvents and the design of CO_2 capture systems, are not considered herein, as it is out of the scope of the present work.

In the case of CO_2 solubility, Henry's constant is typically used as a quick calculation to screen physical solvents. However, a more apt criterion to evaluate solvents based on CO_2 solubility is the solvent cyclic working capacity ($\Delta\alpha_{CO_2}$. The cyclic working capacity, on the basis of moles of CO_2 captured per mole of solvent consumed, is defined as the difference between the amount of CO_2 absorbed in the solvent at absorption conditions and the amount of CO_2 remaining in the solvent at desorption conditions, and it is directly related to the amount of CO_2 effectively captured from the feed flue gas.

$$\Delta\alpha_{CO_2}(T, P) = \alpha_{CO_2}(T, P)_{absorption} - \alpha_{CO_2}(T, P)_{desorption} \tag{6}$$

In the case of effectiveness of mass transfer, the simplest criterion to capture the effect of solvent thermophysical properties on mass transfer would be in terms of diffusion

coefficient of CO_2 (D_{CO_2}), as it is inherently and inversely related to the viscosity of the solvent. A variety of methods are available in the literature for the prediction of diffusion coefficient of CO_2 from thermophysical properties of solvents,[91,92] yet in this work, the diffusion coefficient of CO_2 is determined using the Wilke-Chang expression,[93] expressed as

$$D_{CO_2} = 7.4 \times 10^{-8} \frac{(\varphi MW_{solvent})^{0.5} T}{\mu V_{m,CO_2}^{0.6}} \tag{7}$$

where D_{CO_2} is the diffusion coefficient of CO_2 in the examined solvent, MW is the molar mass of the solvent in g mol^{-1}, μ is the viscosity of the solvent in cP, V_m is the molar volume of CO_2 in cm$^3\cdot$g^{-1}, and φ is the interaction parameter with a value of 7.5 for ILs.[91,92] We have assumed that the same interaction parameter applies to DESs, as they are analogues to ILs.

Evaluating the energy consumption required for solvent regeneration is the last key factor in evaluating the performance of solvents for CO_2 capture. As previously mentioned, the performance of the examined ILs and DESs for CO_2 capture is evaluated using a PSA process at $T = 298$ K. The energy consumption for solvent regeneration (Q) using a PSA process, for which the temperature of absorption and desorption is constant, is expressed as[33,44,48,49,94,95]

$$Q = Q^{des} + Q^{ex} \tag{8a}$$

$$Q^{des} = -H^{dis}(T_{des}, P_{des}) \tag{8b}$$

$$Q^{ex} = \Delta H^{ex} \tag{8c}$$

where, Q^{des} is the energy consumed to vaporize CO_2 from liquid to vapor phase at the desorption conditions, which is the same as the enthalpy of dissolution (H^{dis}). Q^{ex} is the energy consumption due to the difference of excess enthalpy (ΔH^{ex}) between the streams at absorption and desorption conditions. It was previously demonstrated,[44] that the contribution of the energy consumption due to excess enthalpy was generally less than 5%, effectively simplifying the energy needed for solvent regeneration to be fully dependent on the enthalpy of dissolution, which can be derived from the Clausius−Clapeyron equation using information obtained from the soft-SAFT EoS, as

Table 1. Summary of the Ionic Liquids and Deep Eutectic Solvents Examined in This Work[a]

ionic liquids (ILs)[b]	CASRN	cation	anion
1-butyl-3-methylimidazolium tetrafluoroborate $[C_4\,mim][BF_4]$	174501-65-6	$[C_4\,mim]^+$	$[BF_4]^-$
1-butyl-3-methylimidazolium hexafluorophosphate $[C_4\,mim][PF_6]$	174501-64-5	$[C_4\,mim]^+$	$[PF_6]^-$
1-ethyl-3-methylimidazolium bis(trifluoromethylsufonyl)imide $[C_2\,mim][NTf_2]$	174899-82-2	$[C_2\,mim]^+$	$[NTf_2]^-$
1-butyl-3-methylimidazolium bis(trifluoromethylsufonyl)imide $[C_4\,mim][NTf_2]$	174899-82-3	$[C_4\,mim]^+$	$[NTf_2]^-$
1-butylpyridinum bis(trifluoromethylsufonyl)imide $[C_4\,py][NTf_2]$	187863-42-9	$[C_4\,py]^+$	$[NTf_2]^-$
1-hexyl-3-methylpyridinum bis(trifluoromethylsufonyl)imide $[C_6\,mpy][NTf_2]$	547718-92-3	$[C_6\,mpy]^+$	$[NTf_2]^-$
1-butyl-3-methylimidazolium thiocyanate $[C_4\,mim][SCN]$	344790-87-0	$[C_4\,mim]^+$	$[SCN]^-$
1-butyl-3-methylimidazolium methyl sulfate $[C_4\,mim][MeSO_4]$	401788-98-5	$[C_4\,mim]^+$	$[MeSO_4]^-$
1-hexyl-3-methylimidazolium chloride $[C_6\,mim][Cl]$	171058-17-9	$[C_6\,mim]^+$	$[Cl]^-$
1-ethyl-3-methylimidazolium perfluorobutanesulfonate $[C_2\,mim][C_4F_9SO_3]$	NA	$[C_2\,mim]^+$	$[C_4F_9SO_3]^-$
1-butyl-3-methylimidazolium perfluorobutanesulfonate $[C_4\,mim][C_4F_9SO_3]$	NA	$[C_4\,mim]^+$	$[C_4F_9SO_3]^-$
1-ethyl-3-methylimidazolium trifluoromethanesulfonate $[C_2\,mim][CF_3SO_3]$	145022-44-2	$[C_2\,mim]^+$	$[CF_3SO_3]^-$
1-ethyl-3-methylimidazolium trifluoroacetate $[C_2\,mim][CF_3CO_2]$	174899-65-1	$[C_2\,mim]^+$	$[CF_3CO_2]^-$
1-ethyl-3-methylimidazolium bis(perfluoroethylsulfonyl)imide $[C_2\,mim][N(C_2F_5SO_2)_2]$	216299-76-2	$[C_2\,mim]^+$	$[N(C_2F_5SO_2)_2]^-$
deep eutectic solvents (DESs)[c]	CASRN	HBA	HBD
tetra-methyl ammonium chloride/lactic acid $[TMA][Cl]$/LA (1:2)	(75-57-0): (50-21-5)	$[TMA][Cl]$	LA
tetra-ethyl ammonium chloride/lactic acid $[TEA][Cl]$/LA (1:2)	(56-34-8): (50-21-5)	$[TEA][Cl]$	LA
tetra-butyl ammonium chloride/lactic acid $[TBA][Cl]$/LA (1:2)	(1112-67-0): (50-21-5)	$[TBA][Cl]$	LA
tetra-ethyl ammonium bromide/levulinic acid $[TEA][Br]$/LevA (1:3)	(71-91-0): (123-76-2)	$[TEA][Br]$	LevA
tetra-butyl ammonium bromide/levulinic acid $[TEA][Br]$/LevA (1:3)	(1643-19-2): (123-76-2)	$[TBA][Br]$	LevA
choline chloride/ethylene glycol $[Ch][Cl]$/EG (1:2)	(67-48-1): (107-21-1)	$[Ch][Cl]$	EG
choline chloride/glycerol $[Ch][Cl]$/GLY (1:2)	(67-48-1): (56-81-5)	$[Ch][Cl]$	GLY

[a]The cation and anion refer to the components for the ILs, while HBD and HBA refer to those for DESs. [b]Modeled as a single substance using the *pseudopure component* approach. [c]Modeled as a binary mixture of the individual components using the *individual-component* approach.

$$-H^{dis} \approx -H^{abs} = H^{des} = R\left(\frac{\partial \ln P_i^{vap}}{\partial(1/T)}\right)_{x_i} \quad (9)$$

It should be noted, that the negative value of the enthalpy of absorption is equal to the enthalpy of desorption.

Coarse-Grain soft-SAFT Molecular Models of Ionic Liquids and Deep Eutectic Solvents. The key step in applying SAFT-based EoSs to real fluids is the proposition of a simplified coarse-grain molecular model of the examined fluid, capturing its basic structural and energetic features. Following our previous work, carbon dioxide was modeled as a homonuclear chainlike LJ fluid, explicitly considering its quadrupole moment. The fraction of quadrupolar segments was fixed a priori, $(x_p = \frac{1}{3})$, based on the geometry of the molecule, while its quadrupole moment was included in the fitting procedure, yielding a value relatively similar to the experimental one.[96,97]

The development of coarse-grain molecular models for ILs and DESs is relatively similar due to their parallel molecular nature, being mixtures of individual components/species bounded by some form of physical strong and highly directional interactions, well captured by the association term in SAFT-type equations. For these substances, the mixture of their individual components can be modeled either as a single substance (*pseudopure component* approach), or as a binary mixture of the individual components (*individual-component* approach).[10,11,98] A graphical representation of the soft-SAFT molecular models for selected ILs and DESs examined in this work is depicted in Figure 1. Additionally, a summary of the ILs and DESs modeled is included in Table 1.

The ILs were modeled using the *pseudopure component* approach as associating single chainlike fluids with the attractive interactions between the counterions mimicked through the addition of specific association sites (defined a

priori) dependent on the structure and charge distribution of the IL. For ILs with $[BF_4]^-$, $[PF_6]^-$, $[Cl]^-$, $[CF_3SO_3]^-$, and $[CF_3CO_2]^-$ anions, a single association site of type A was included in their models as the neutral counterions pair is quasi-spherical with a very localized charge, with A–A interactions allowed in the model due to the dual nature of the association site.[68,73,99] Alternatively, $[C_4\,mim][MeSO_4]$ and $[C4mim][SCN]$ were modeled with two association sites, one site of type A representing the interaction between the anion and the cation, and one site of type B, mimicking the delocalized charge due to the oxygen molecule on the anion, with only A–B interactions allowed in the model.[99,100] In a similar fashion, ILs with $[NTf_2]^-$, $[C_4F_9SO_3]^-$, and $[N-(C_2F_5SO_2)_2]^-$ anions were modeled with three association sites, one site of type A and two sites of type B, as a consequence of a higher degree of charge delocalization in the anion, again only allowing A–B interactions in the model.[69,72,73] The soft-SAFT molecular parameters for the examined ILs were transferred from previous contributions,[68,69,72,73,99,101] and are included in Table S1 in the Supporting Information for completeness.

The DESs were modeled using the *individual-component* approach.[11] In this manner, each individual component is characterized by a separate set of parameters and an additional binary interaction parameter accounting for deviations in size or energy between both components. The hydrogen-bond acceptors (HBAs) such as tetraalkylammonium chloride salts $[TXA][Cl]$,[11] and tetraalkylammonium bromide salts $[TXA]-[Br]$,[77] were modeled as associating fluids with two association sites, one negative and one positive site, mimicking the anion–cation interactions. For the highly complex choline chloride salt $[Ch][Cl]$,[78] a more rigorous model was developed, guided by molecular dynamic simulations, with five association sites: (1) one of type H and one of type e, mimicking the hydroxyl group with association parameters transferred from 1-
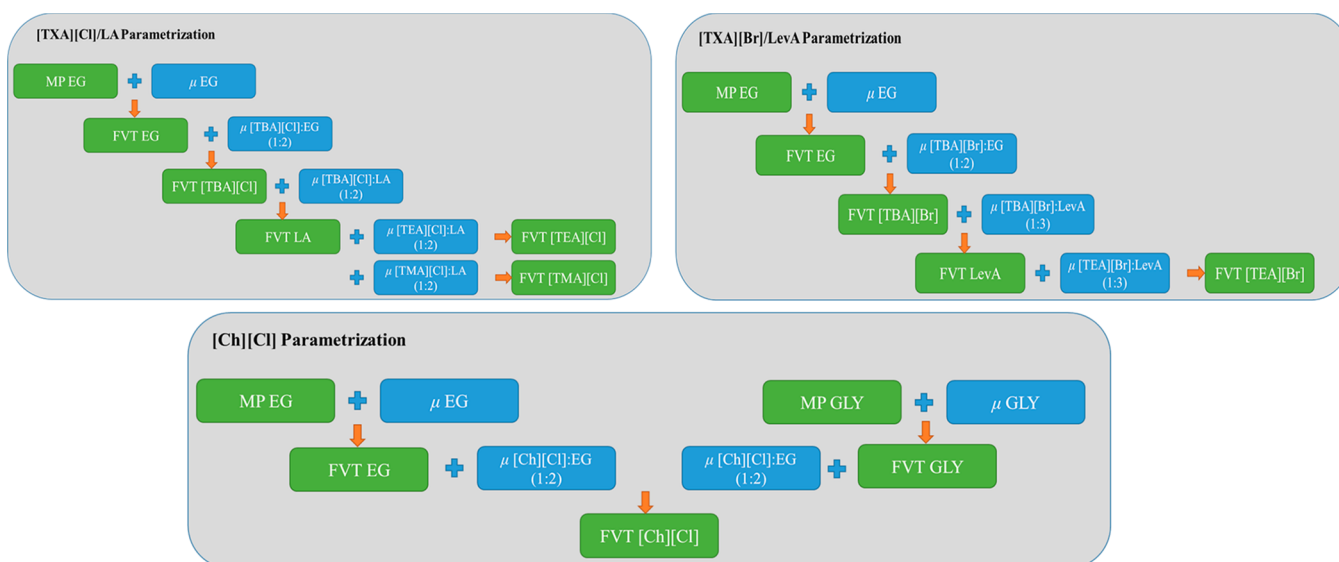
Figure 2. Schematic procedure for the sequence of parametrizing free-volume theory (FVT) parameters to describe the viscosity of the individual components of pure DESs examined in this work. The green boxes refer to either molecular parameters (MP), or FVT parameters of the examined substances, included in Tables S1 and S2 in the Supporting Information, while the blue boxes refer to experimental viscosity data (μ) for the examined pure fluid (EG) or DES. See notation in Table 1.

propanol; (2) one pair of negative and positive sites mimicking the cation–anion interactions transferred from the interactions of tetraalkylammonium chloride salts;[76] and (3) one additional site representing the hydrogen-bond donor character of the methyl groups, predicted from combining rules. The hydrogen-bond donors (HBDs) were modeled as associating chainlike fluids with two association sites. The binary size interaction parameter (η) was fitted to available binary mixture liquid density data to accurately capture the behavior of the binary mixture, as this is the data available in most of the cases.[76,77] See the work of Crespo and co-workers[78] for the inclusion of solid–liquid equilibria (SLE) to appropriately capture the intermolecular interactions for [Ch][Cl]/EG and [Ch][Cl]/GLY DESs. The molecular parameters for the individual components of DESs examined in this work, and their binary interaction parameters, were transferred from previous contributions,[76–78] and included in Table S1 in the Supporting Information for completeness.

■ RESULTS AND DISCUSSIONS

In this section, we present the application of the soft-SAFT EoS for the screening of ILs and DESs, for the physical absorption of CO_2. The soft-SAFT calculations for the thermophysical properties of the pure solvents and their phase equilibria with CO_2 are validated against experimental data with the molecular parameters of the pure solvents transferred from previous contributions.[68,69,72,76–78,99,100,102] The models are subsequently used in a predictive manner to assess the potentiality of these solvents in terms of KPIs such as cyclic working capacity, enthalpy of absorption, and diffusivity, capturing the trade-offs between these properties on the effectiveness of ILs and DESs for CO_2 capture.

Viscosity Calculations of pure ILs and DESs. The description of the liquid density at atmospheric pressure for the pure solvents as obtained from soft-SAFT with the transferred molecular parameters, compared to experimental data for ILs[72,99,103–107] and DESs[108–111] is shown in Figure S1

in the Supporting Information, highlighting the quantitative accuracy of the models used in this work for ILs and DESs.

The viscosities of the examined solvents were obtained in this work using the FVT treatment combined with soft-SAFT, requiring three additional molecular parameters regressed using pure viscosity experimental data. The FVT treatment parametrization procedure for ILs is straightforward, modeled using the *pseudopure component* approach, fitting the FVT parameters to available viscosity experimental data of pure ILs, using the previously regressed soft-SAFT molecular parameters provided in Table S1 in the Supporting Information. In the case of DESs, modeled using the *individual-component* approach as binary mixtures, the fitting procedure was modified, as some of the individual components are solid at a wide range of conditions, with no experimental viscosity data. Hence, the spider-web methodology[112] was utilized to fit the FVT parameters for the solid components of the examined DESs. With this approach, the FVT parameters were fitted simultaneously to the viscosity of pure compounds and mixtures, assuming the FVT parameters of one of the compounds (i.e., EG which is a liquid) in the mixture are available. The sequence for parametrizing the FVT parameters for the individual components in the investigated DESs is shown in Figure 2. It should be noted that the sequence provided in this figure relies on using the previously regressed soft-SAFT molecular parameters in a transferable manner in order to obtain thermodynamic information needed for FVT treatment such as temperature, pressure, and density. Additionally, the optimization for FVT parameters is carried out not only attending to the minimal deviation respect to viscosity data, but also looking for meaningful trends for the compounds of the same family. In this regard, the tetraalkylammonium salts present a linear increase of the barrier energy α and a second-order polynomial and linear decrease of the free-volume overlap B and correlation length L_v, respectively, with the molecular weight. This type of trend is similar to that found in previous contributions for other families of compounds.[90]
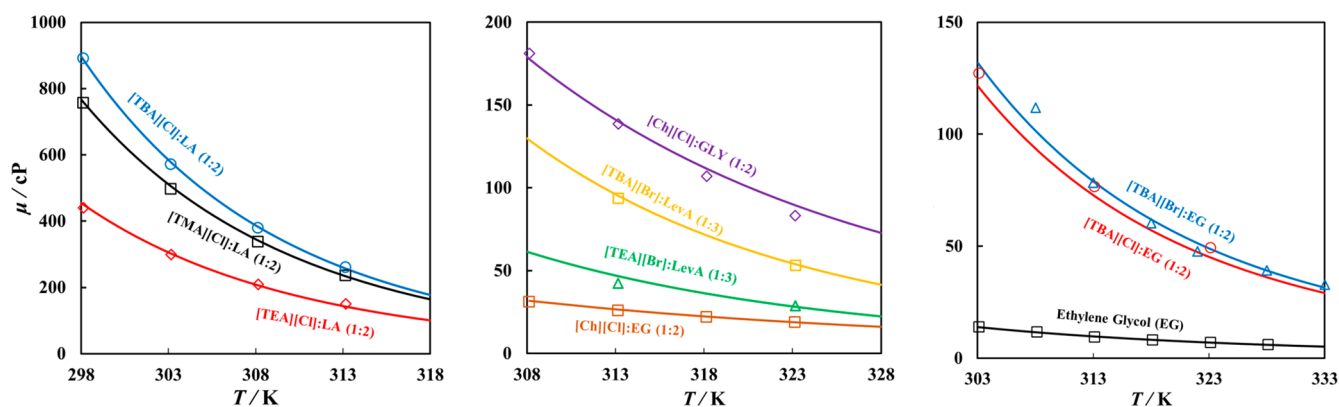
Figure 3. Viscosity of DESs examined in this work at atmospheric pressure, as a function of temperature, modeled using FVT parameters shown in Table S2 in the Supporting Information. Soft-SAFT + FVT calculations (lines) compared to experimental data[113−119] (symbols).
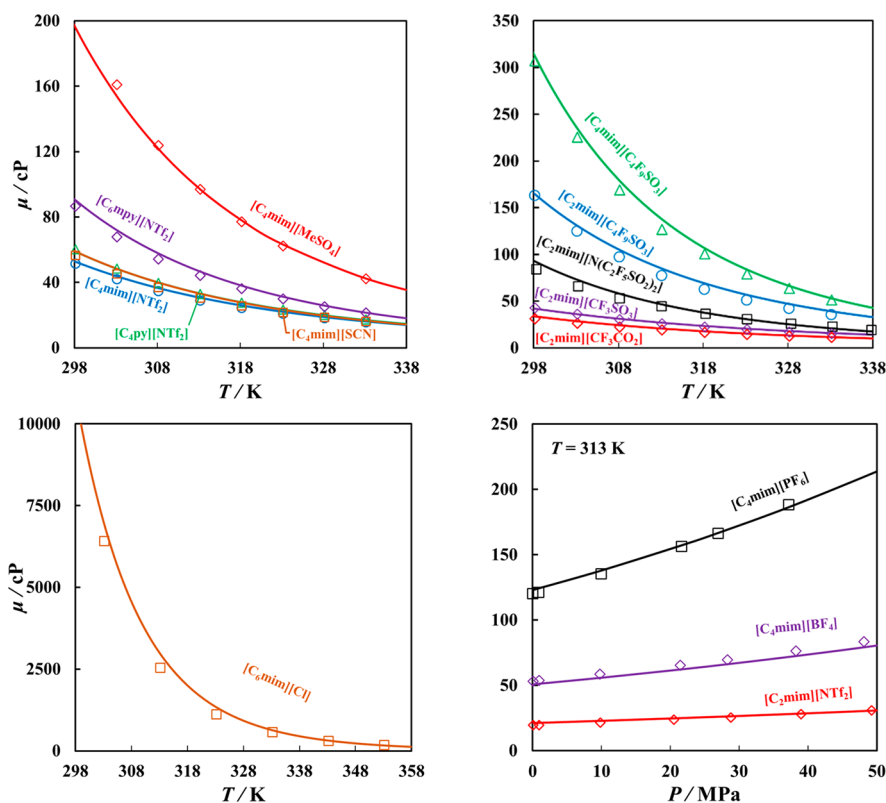

Figure 4. Viscosity of ILs examined in this work as a function of temperature or pressure, modeled using FVT parameters shown in Table S2 in the Supporting Information. Soft-SAFT + FVT calculations (lines) compared to experimental data[106,120−130] (symbols).

With the FVT parameters obtained in this work for ILs and DESs, included in Table S2 in the Supporting Information, the calculations for the pure solvents viscosities from FVT + soft-SAFT are in excellent agreement with experimental data for DESs,[113−119] and ILs[106,120−130] studied in this work, as depicted in Figure 3 and Figure 4, respectively.

Solubility of CO_2 in the Selected ILs and DES. Once the thermodynamic behavior of the pure solvents was assessed, the ability of soft-SAFT in capturing the performance for the solubility of CO_2 in these solvents was studied next. A summary of the binary interaction parameters between CO_2 and ILs, and CO_2 and the individual components of each DES modeled in this work, is included in Table S3 in the Supporting Information, either transferred from previous works[68,71,73,101,102] or developed herein. These binary inter-

action parameters were obtained, when needed, by fitting to an intermediate isotherm and transferred to other conditions in a predictive manner. It should be noted, that in most cases, the binary parameters were fixed to unity, with the CO_2 solubility in these solvents directly predicted from the molecular parameters of the pure fluids (see Table S3), reinforcing the robustness of the soft-SAFT model and the molecular parameters. The soft-SAFT computations for the solubility of CO_2 in ILs and DESs investigated in this work are depicted in Figure 5, validating the robustness of soft-SAFT, accurately capturing the trends for the experimental CO_2 solubility in ILs[107,131−140] and DESs,[111,141−143] respectively.

Evaluation of ILs and DESs for CO_2 Capture. The performance of the selected ILs and DESs for CO_2 capture is evaluated next based on three important factors affecting the
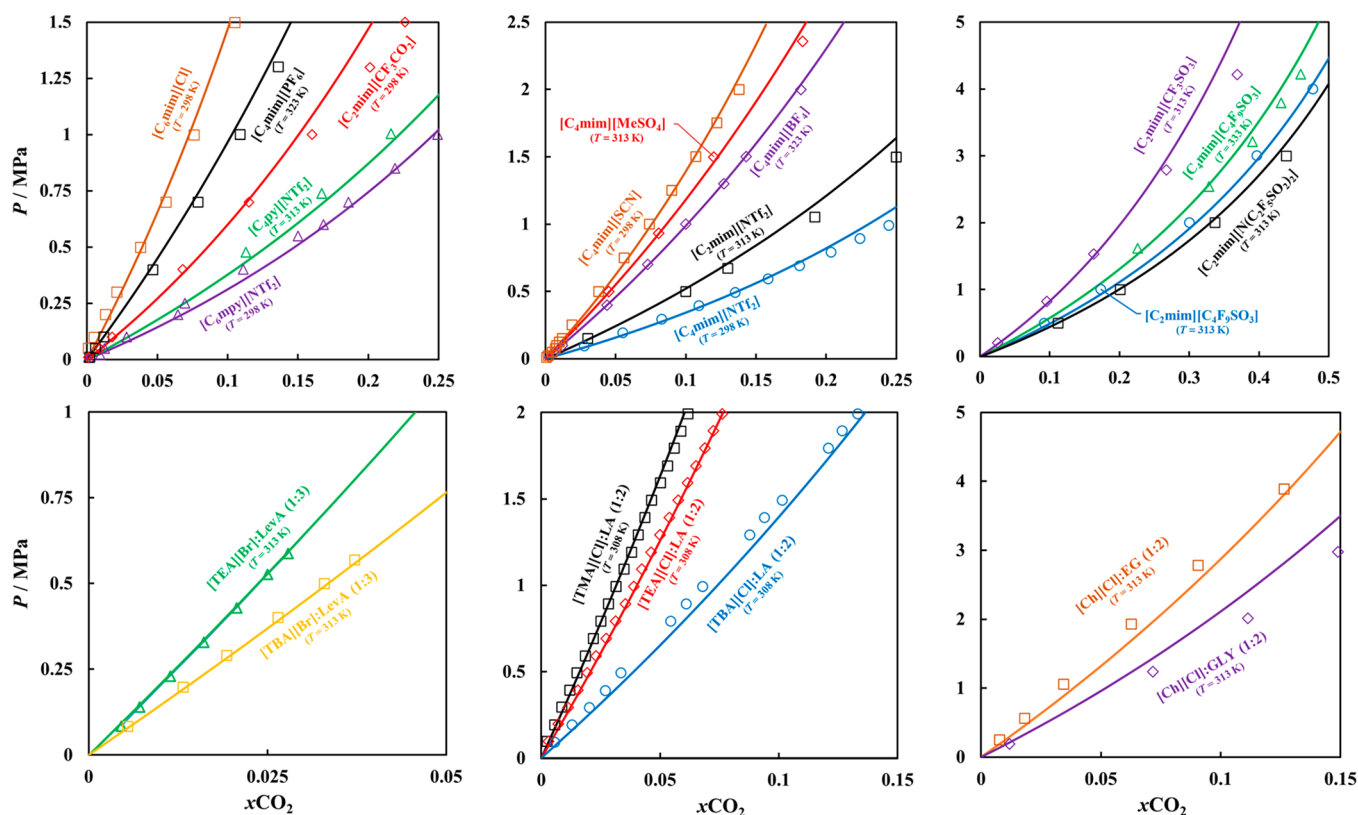
Figure 5. CO_2 solubility in the physical solvents studied in this work, for a variety of ILs depicted in (top), and DESs depicted in (bottom), modeled using binary interaction parameters shown in Table S3 in the Supporting Information. Soft-SAFT calculations (lines) compared to experimental data for CO_2 + ILs,[107,131−140] and for CO_2 + DESs[111,141−143] (symbols).

techno-economic feasibility of CO_2 capture systems, namely, CO_2 absorption capacity, mass transfer, and energy of regeneration. All calculations were performed using soft-SAFT models in a fully predictive manner.

CO_2 Absorption Capacity. One of the key factors in deciding the choice of solvent for CO_2 capture is its affinity to CO_2 as this dictates the efficiency of the solvent in removing CO_2 from the incoming feed gas and has a direct impact on the capital and operating expenditure for the process. Typically, the physical CO_2 absorption process occurs at low temperatures and high pressures; as such, the solubility of CO_2 in the examined solvents was evaluated at $T = 298$ K, and in the pressure range of $P = 0.1−2500$ kPa. The absorption loading, represented as mole of CO_2 per mole of solvent of the examined ILs and DESs, was directly obtained from soft-SAFT in a fully predictive manner, and the results are depicted in Figure 6. It can be observed that, under the same absorption conditions, the majority of the examined ILs, except [C$_6$ mim][Cl] and [C$_4$ mim][SCN], have a higher CO_2 absorption loading than all the examined DESs. Increasing the CO_2 absorption capacity of DESs to be comparable with those obtained for ILs would require a higher operating pressure at the absorption conditions. The highest CO_2 loading capacity, for example at 1000 kPa, was obtained for [C$_4$ py][NTf$_2$] IL with an absorption loading of 0.4 mol $CO_2 \cdot$ mol^{-1} IL. When these solvents are contrasted to traditional aqueous alkanolamines used as physical solvents for CO_2 capture, such as a 30 wt % aqueous methyl diethanolamine (MDEA), or a 20/10 wt % aqueous blend of MDEA and piperazine (PZ), their absorption capacity can reach a loading of 1.25 mol $CO_2 \cdot$ mol^{-1} amine at the same conditions, based on screening results

previously obtained using soft-SAFT EoS.[27] This is almost 3 times higher than that obtained for [C$_4$ py][NTf$_2$]. Please, notice that no comparisons are presented with 30 wt % aqueous MEA or DEA because they are chemical solvents rather than physical; hence their comparison with ILs and DESs will not be fair.

Focusing on the affinity of ILs to CO_2, the highest CO_2 absorbing ILs were [C$_4$ py][NTf$_2$] > [C$_4$ mim][C$_4$F$_9$SO$_3$] > [C$_2$ mim][N(C$_2$F$_5$SO$_2$)$_2$] as seen in Figure 6a−c. For the examined ILs, the solubility of CO_2 is affected by both the chain length and type of the cation, and the type of anion.[3,44] For ILs with the same cation, for example, [C$_2$ mim]$^+$ or [C$_4$ mim]$^+$, depicted in Figure 6a−b, the increase in CO_2 solubility is associated with an increase in the molecular weight of the anion. For [C$_2$ mim]$^+$-based ILs, the increase in CO_2 solubility with the different anions is in the order of [CF$_3$CO$_2$]$^-$ ≈ [CF$_3$SO$_3$]$^-$ < [NTf$_2$]$^-$ < [C$_4$F$_9$SO$_3$]$^-$ < [N(C$_2$F$_5$SO$_2$)$_2$]$^-$, while that for [C$_4$ mim]$^+$-based ILs is in the order of [SCN]$^-$ < [MeSO$_4$]$^-$ < [BF$_4$]$^-$ ≈ [PF$_6$]$^-$ < [NTf$_2$]$^-$ < [C$_4$F$_9$SO$_3$]$^-$. Similarly, the type and chain length of the cation has an impact on the solubility of CO_2. For [NTf$_2$]$^-$ and [C$_4$F$_9$SO$_3$]$^-$-based ILs, it was observed that increasing the chain length of the cation from [C$_2$ mim]$^+$ to [C$_4$ mim]$^+$, marginally increased the solubility of CO_2 in these ILs approximately by 6%. Conversely, the effect of the type of cation on CO_2 solubility was more appreciable, as observed for [NTf$_2$]$^-$ based ILs. By changing the type of cation from imidazolium (i.e., [C$_2$ mim]$^+$ and [C$_4$ mim]$^+$) to pyridinum (i.e., [C$_4$ py]$^+$ and [C$_6$ mpy]$^+$), CO_2 solubility increased by approximately 38% and 15%, respectively, with [C$_2$ mim][NTf$_2$] being the reference point.
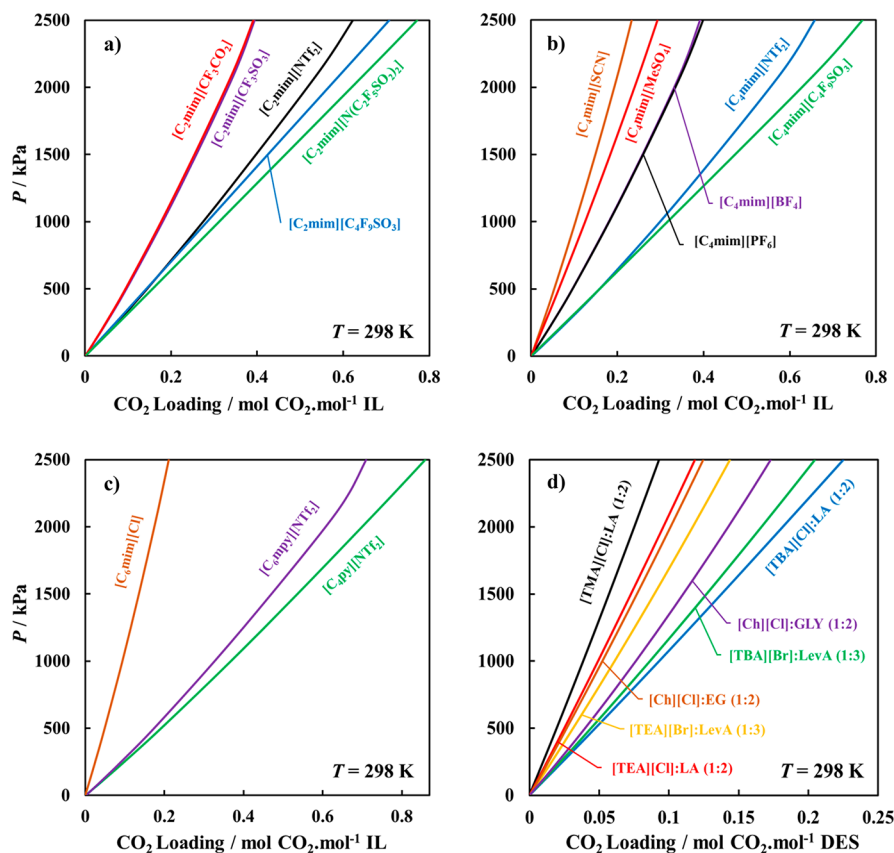
Figure 6. CO_2 loading at $T = 298$ K as a function of pressure from 0.1 to 2500 kPa in (a) ethyl-imidazolium ([C_2 mim]) ILs, (b) butyl-imidazolium ([C_4 mim]) ILs, (c) other ILs, and (d) a variety of DESs, as predicted from soft-SAFT (lines).

In the case of DESs, the highest CO_2 loading was observed for [TBA][Br]/LevA (1:3) and [TBA][Cl]/LA (1:2), as shown in Figure 6d. The CO_2 solubility in DESs is also affected by the type of HBD and HBA, analogues to the cation and anion in ILs. For the same HBD, for example, LA and LevA, increasing the chain length of the HBA from tetraethylammonium halide salt to tetrabutylammonium halide almost doubled the CO_2 solubility in the examined DESs. In contrast, for the same HBA, for example, choline chloride [Ch][Cl], the choice of HBD had an effect on the CO_2 solubility with [Ch][Cl]/GLY having twice the absorption capacity of [Ch][Cl]/EG. This might be related to the CO_2 solubility in the pure HBD, as glycerol has a higher CO_2 solubility than ethylene glycol. It should be noted that the conclusions drawn here on the effect of the individual components of DESs on CO_2 solubility are only based on the solvents examined in this work. A larger variety of DESs at different molar ratios should be studied to provide more insights.

The cyclic working capacity of each solvent examined in this work was determined using eq 6. The chosen absorption conditions are $T = 298$ K and two operating pressures, at 1000 and 2500 kPa, to examine the effect of absorption conditions on cyclic working capacity, while the chosen desorption conditions are $T = 298$ K and $P = 10$ kPa. Moreover, the amount of solvent required for CO_2 capture at these conditions has been evaluated on the basis of tons of solvent per ton of CO_2. These results were obtained from the predictions shown in Figure 6 using soft-SAFT EoS. Depicted in Figure 7a,b, are the cyclic working capacity and solvent
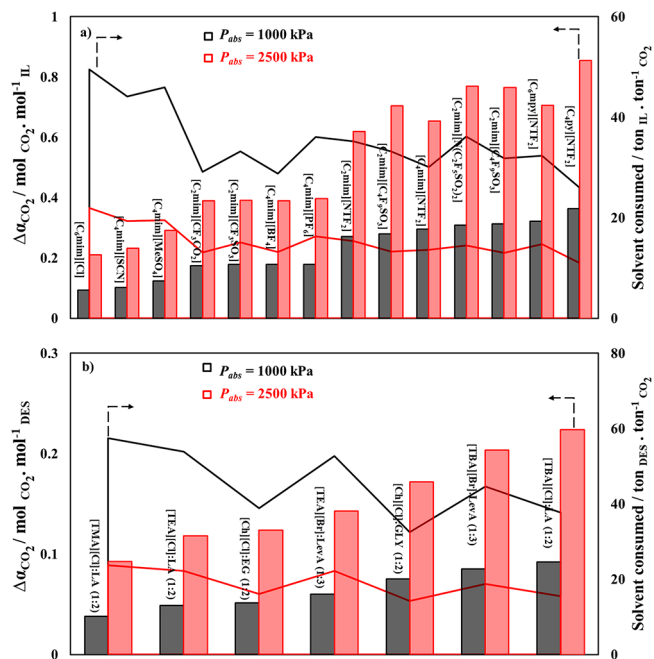
Figure 7. Solvent cyclic working capacity at $T = 298$ K (bars) and solvent consumption (lines) for (a) ILs, and (b) DESs, with the red color denoting absorption at $P = 2500$ kPa, while black denotes absorption at $P = 1000$ kPa. In both cases, it was assumed that the solvent regeneration occurred at $T = 298$ K and $P = 10$ kPa.

consumption for the examined ILs and DESs. It is observed that increasing the absorption operating pressure from 1000 to
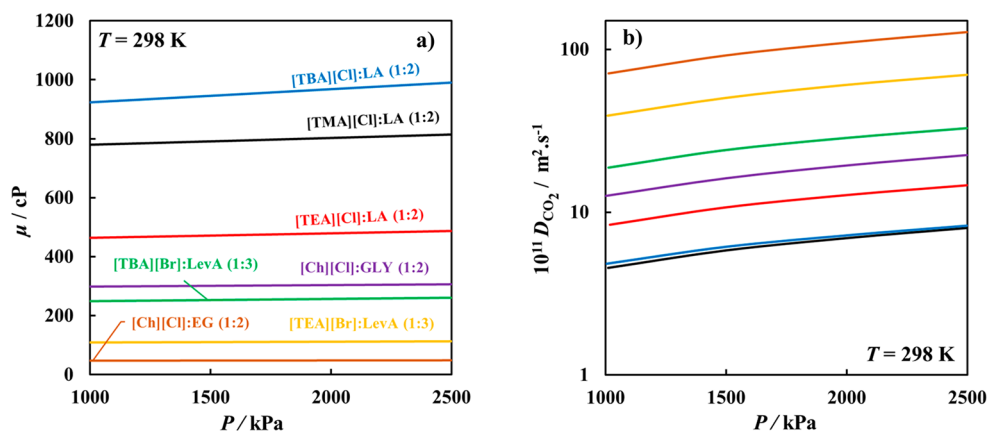
Figure 8. a) Viscosity of pure DESs and (b) diffusion coefficients of CO_2 in DESs at $T = 298$ K as a function of the absorption operating pressure for DESs, as predicted from soft-SAFT and Wilke-Chang expression for the diffusion coefficient[93] (lines).

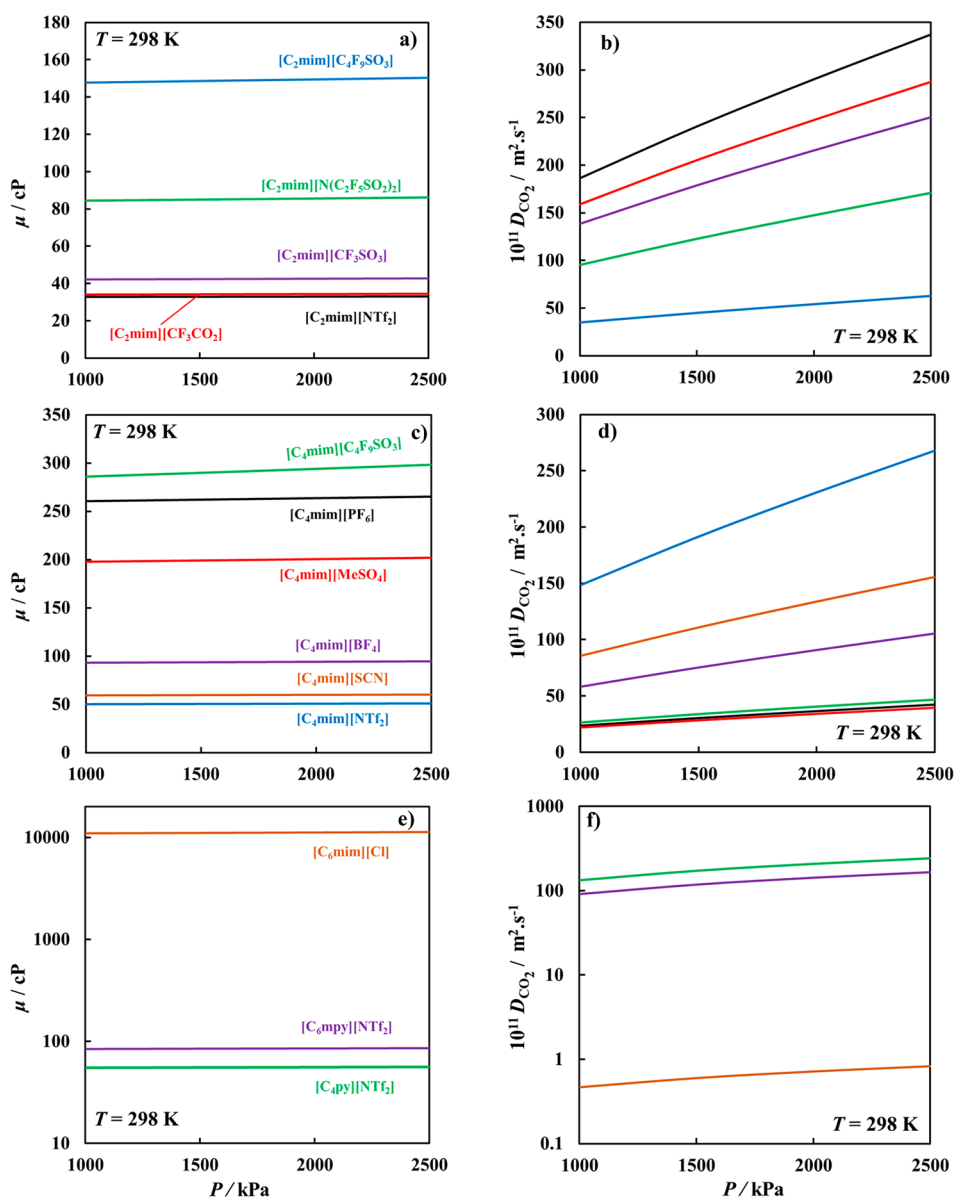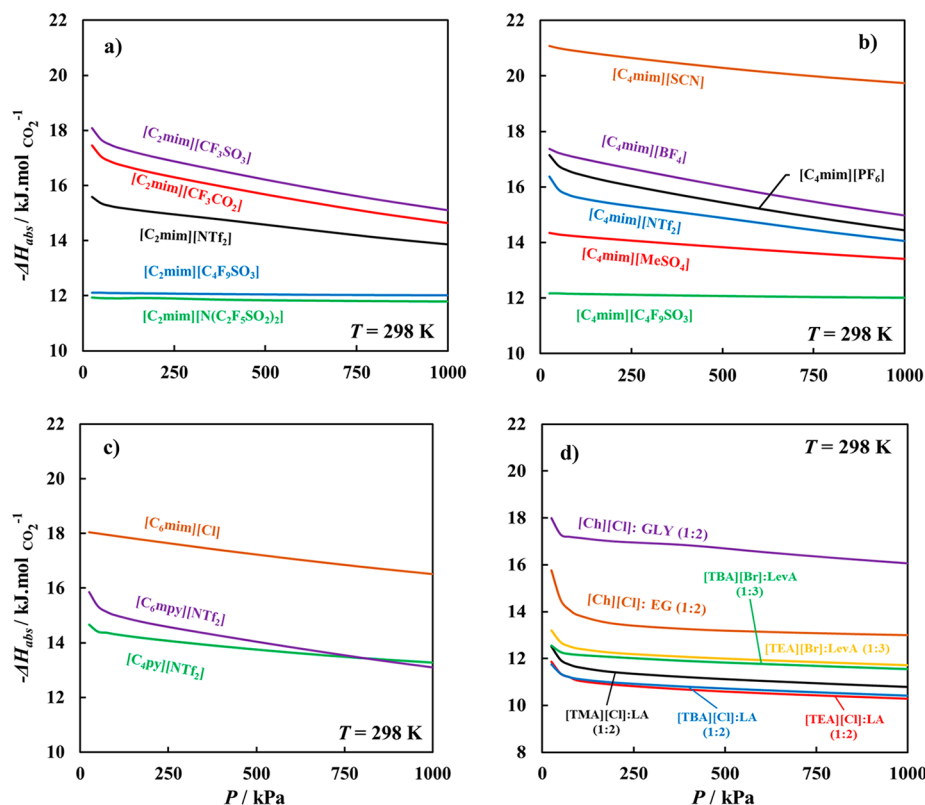**Figure 9.** Viscosity of pure ILs and diffusion coefficients of CO_2 in examined ILs at $T = 298$ K as a function of the absorption operating pressure for (a,b) ethyl-imidazolium ILs, (c,d) butyl-imidazolium ILs, and (e,f) other ILs, as predicted from soft-SAFT and Wilke-Chang expression for the diffusion coefficient[93] (lines).

Figure 10. Enthalpy of desorption at T = 298 K as a function of desorption pressure in (a) ethyl-imidazolium ILs, (b) ethyl-imidazolium ILs, (c) other ILs, and (d) a variety of DESs as predicted from soft-SAFT (solid lines).

2500 kPa resulted in an increase in the cyclic working capacity of all the examined solvents, ranging from 19% to 51% dependent on the type of IL, and in the range of 28% to 43% dependent on the type of DES. The largest cyclic capacity was observed for $[C_4 py][NTf_2]$ with 0.36 and 0.85 mol CO_2·mol^{-1} IL, at 1000 and 2500 kPa, respectively, while the largest cyclic capacity for the DESs was obtained for $[TBA][Cl]/LA$ (1:2) with 0.092 and 0.224 mol CO_2·mol^{-1} DES at the same conditions. In terms of solvent consumption, an inverse relationship exists with the cyclic working capacity in which the higher are the operating pressure and cyclic working capacity, the lower is the amount of solvent required/used. The IL $[C_4 py][NTf_2]$ had the lowest solvent consumption with 26.0 and 11.0 tons required to capture 1 ton of CO_2, at 1000 and 2500 kPa, respectively. Similarly, capturing 1 ton of CO_2 using $[TBA][Cl]/LA$ (1:2) would require 37.6 and 15.4 tons of the solvent at the same conditions.

The cyclic working capacity and solvent consumption for $[C_4 py][NTf_2]$ and $[TBA][Cl]/LA$ (1:2), at T = 298 K, P_{abs} = 1000 kPa, and P_{des} = 10 kPa, is compared to that for traditional aqueous alkanolamines. On the bais of results from a previous contribution,[27] the cyclic working capacity of 30 wt % aqueous MDEA, and a 20/10 wt % aqueous blend of MDEA + PZ at those conditions are *ca.* 0.55 and 0.75 mol CO_2·mol^{-1} amine, respectively, while the amount of alkanolamine consumed to capture 1 ton of CO_2 is 4.97 and 0.98 tons. These values are far more superior to those obtained for the promising IL and DES. This demonstrates that the feasibility of these alternative solvents is not in terms of amount of CO_2 captured, so reaching a level comparable to that obtained with aqueous alkanolamines would require a higher operating pressure to increase the amount of CO_2 captured. Yet, this is not

necessarily a negative point, as it is observed that the physical absorption process with these solvents tends to become more efficient at higher absorption operating pressures, by increasing the amount of CO_2 captured and decreasing the amount of solvent consumed. This will have direct implications on the capital costs of the processing units and operating costs for heating and cooling requirements being reduced due to the lower solvent flow rate.[25,46] In contrast, the effect of increasing the absorption operating pressure will manifest in increased sizing and utility consumption of the compression unit, which has been demonstrated to be dependent on the operating conditions rather than the type of solvent.[46]

Effect on Mass Transfer. Mass transfer is another vital processing aspect of key importance for the design of CO_2 capture units, due to its effect on the capital cost associated with the height of the absorption column. The inclusion of this factor is typically neglected in assessments based on equilibrium and energy balances of the process. The work of Mota-Martinez and co-workers[25,46] established that diffusivity and viscosity are among the most important thermodynamic properties directly impacting the design of the column based on the effectiveness of mass transfer. The effect of viscosity on the economics of the process has a higher contribution to the capital cost in terms of height of the absorber, than the operating cost in terms of energy required for solvent pumping.

All the required thermophysical properties to predict the diffusion coefficient of CO_2 in ILs and DESs, using eq 7, have been obtained from soft-SAFT at T = 298 K, and in the absorption pressure range of 1000 to 2500 kPa, to examine the effect of absorption pressure on pure solvent viscosity and CO_2 diffusivity in the solvent, as depicted in Figure 8 and Figure 9. The effect of the absorption operating pressure on the viscosity
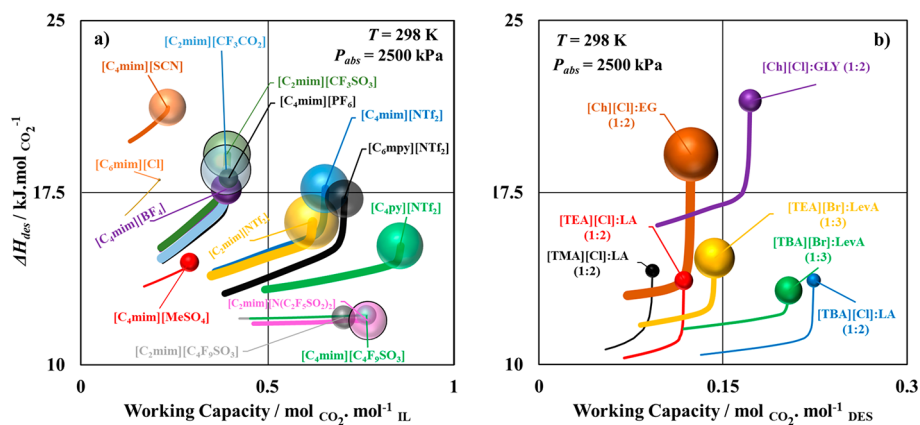
Figure 11. Comparative assessment of (a) ILs, and (b) DESs examined in this work for CO_2 absorption. All calculations were obtained from soft-SAFT at T = 298 K, P_{abs} = 2500 kPa, and P_{des} = 10−1000 kPa (lines from right to left). See text for details.

of pure ILs and DESs is negligible as they are incompressible fluids, while the effect on the CO_2 diffusion coefficient in the examined solvents is more pronounced. The increase in the diffusion coefficient at higher absorption operating pressures implies an enhancement in the mass transfer of CO_2 and its absorption in these solvents. This will reflect on the design of the absorption column being smaller in size and subsequently reducing the capital expenditure, which has also been previously demonstrated in the case of increased cyclic working capacity. Moreover, it can be seen that the higher is the viscosity of the solvent, the lower is its CO_2 diffusion coefficient. The highest CO_2 diffusion coefficient was obtained for all $[NTf_2]^-$-based ILs, irrespective of the cation part, and for [Ch][Cl]/EG (1:2), and [TEA][Br]/LevA (1:3) DESs.

Energy of Regeneration. The energy of desorption required for regenerating ILs and DESs examined in this work has been evaluated, using eq 9, at T = 298 K, and in the pressure range of 10−1000 kPa, to investigate the effect of desorption pressure on the desorption enthalpy, as shown in Figure 10. It is observed that for all the examined solvents, increasing the desorption pressure resulted in a reduction in the magnitude of the enthalpy of absorption. Thus, at higher regenerator operating pressures, the energy required for solvent regeneration would be lower; however, the amount of CO_2 recovered would also decrease.

The lowest enthalpy of desorption is observed for the ILs $[C_2 mim][N(C_2F_5SO_2)_2]$ < $[C_2 mim][C_4F_9SO_3]$ < $[C_4 mim]$ $[C_4F_9SO_3]$ and for the DESs [TBA][Cl]/LA (1:2) ≈ [TEA][Cl]/LA (1:2), approximately in the magnitude of 12 $kJ \cdot mol^{-1}$ CO_2 as seen in Figure 10a−d. As shown in Figure 10 panels a−c, the effect of the anion and cation on the enthalpy of desorption for ILs was isolated allowing quantification of the influence of each of them on their final performance for this KPI. Examining the effect of the anion for ILs with $[C_2 mim]^+$ and $[C_4 mim]^+$ cations shows that the enthalpy of desorption decreases with increasing molecular weight of the anion, or alternatively, decreasing relatively in the same order of anions that presented an increase in the CO_2 solubility shown in Figure 6a,b. For $[C_2 mim]^+$-based ILs, the absolute enthalpy of desorption with the different anions is in the order of $[CF_3SO_3]^-$ > $[CF_3CO_2]^-$ > $[NTf_2]^-$ > $[C_4F_9SO_3]^-$ > $[N(C_2F_5SO_2)_2]^-$, while that for $[C_4 mim]^+$-based ILs is in the order of $[SCN]^-$ > $[BF_4]^-$ > $[PF_6]^-$ > $]^-$ < $[NTf_2]^-$ > $]^-$ < $[MeSO_4]^-$ > $[C_4F_9SO_3]^-$. Similarly, the type and chain length of the cation has an impact on the enthalpy of desorption. For

$[NTf_2]^-$ and $[C_4F_9SO_3]^-$-based ILs, it was observed that increasing the chain length of the cation from $[C_2 mim]^+$ to $[C_4 mim]^+$ marginally increased the enthalpy of desorption in these ILs. In contrast, the effect of the type of cation on CO_2 solubility was more appreciable, as observed for $[NTf_2]^-$ based ILs. Changing the type of cation from imidazolium (i.e., $[C_2 mim]^+$ and $[C_4 mim]^+$) to pyridinum (i.e., $[C_4 py]^+$ and $[C_6 mpy]^+$), resulted in a more pronounced reduction in the enthalpy of desorption.

In this aspect, the advantage of ILs and DESs compared to conventional aqueous alkanolamines manifests itself. The enthalpy of desorption for a 30 wt % aqueous MDEA solution is 52.5 $kJ \cdot mol^{-1}$ CO_2,[144] being four times higher than that observed for ILs and DESs with the lowest desorption enthalpy examined in this work. Additionally, the presence of large quantities of water as a cosolvent with alkanolamines adds a parasitic load on the amount of energy required for regeneration due to the high heat capacity and enthalpy of vaporization of water.[29]

Comparative Assessment of ILs and DESs for CO_2 Capture. The effective assessment for the potentiality of ILs and DESs examined in this work for CO_2 capture requires taking into account trade-offs between the selected KPIs, namely, cyclic working capacity, CO_2 diffusion coefficient, and enthalpy of desorption, due to their influence on capital and operating costs, as previously highlighted. The solvent performance is assessed at T = 298 K and P = 2500 kPa for absorption, while the desorption occurs at T = 298 K, and in the pressure range of 10−1000 kPa. Provided in Figure 11 is the comparative assessment of ILs and DESs for CO_2 capture based on the chosen selection criteria; the optimal solvents would be those with a high cyclic working capacity, low enthalpy of desorption, and high CO_2 diffusion coefficient. The thick lines reflect the evolution of cyclic working capacity and enthalpy of desorption with a change in the desorption pressure from 10−1000 kPa, with the large spheres at the end of the line denoting desorption at 10 kPa. Moreover, the size of the sphere denotes the magnitude of the CO_2 diffusion coefficient in these solvents: the larger the better.

For the examined ILs as shown in Figure 11a, it is observed that the solvents with high working capacity and low enthalpy of desorption are $[NTf_2]^-$-based ILs (i.e., $[C_4 py]^+$, $[C_2 mim]^+$, $[C_4 mim]^+$, and $[C_6 mpy]^+$), $[C_2 mim][N(C_2F_5SO_2)_2]$, $[C_2 mim][C_4F_9SO_3]$, and $[C_4 mim][C_4F_9SO_3]$. With the inclusion on the mass transfer effect in the form of CO_2 diffusion

coefficient (size of the bubble), it can be seen that ILs with $[N(C_2F_5SO_2)_2]^-$ and $[C_4F_9SO_3]^-$ anions have a poor transfer rate due to their low CO_2 diffusion coefficient, resulting in a larger absorption column. Considering the trade-offs between the three selection criteria, the most promising IL is $[C_4 py][NTf_2]$ as it shows the highest cyclic working capacity, relatively low enthalpy of desorption, and high CO_2 diffusion coefficient compared to the other ILs, while the least promising is $[C_6 mim][Cl]$ due to its extremely large viscosity and low CO_2 diffusion coefficient. Another important observation is that, with decreasing the desorption pressure, the cyclic working capacity increases with increasing enthalpy of desorption until reaching a critical desorption pressure, where the increase in enthalpy of desorption outweighs the additional increase in the working capacity, as shown by the nearly horizontal lines when the operating pressure approaches 10 kPa.

Similarly, for the examined DESs shown in Figure 11b, the most promising solvents in terms of working capacity and enthalpy of desorption are both LevA-based DESs and $[TBA][Cl]/LA$ (1:2). However, including the effect on mass transfer revealed that only $[TEA][Br]/LevA$ (1:3) would be viable for CO_2 capture, due to its higher CO_2 diffusion coefficient. The effect of the desorption pressure on the change of working capacity and enthalpy of desorption, similar to that observed with ILs, is more pronounced in the case of DESs.

Lastly, comparing the promising solvents from both categories ($[C_4 py][NTf_2]$ from ILs, and $[TEA][Br]:LevA$ (1:3) from DESs), it is demonstrated that both solvents have a relatively similar enthalpy of desorption, nevertheless, $[C_4 py][NTf_2]$ outperformed the DES with approximately 5.5 times the amount of CO_2 captured, and 7 times higher CO_2 diffusion coefficient, indicating that this solvent is far more efficient than the best performing DES. In fact, the majority of the examined ILs, even the poorest ones, have a better performance than the best DES in terms of working capacity.

CONCLUSIONS

In this work, the soft-SAFT EoS has been employed as a reliable platform for the screening of a variety of ionic liquids and deep eutectic solvents as physical solvents for CO_2 capture. The models for the pure solvents and their binary mixtures with CO_2 have been validated against available experimental data, using previously developed molecular models for the examined compounds. Subsequently, the models were used in a fully predictive manner to assess the performance of these solvents in terms of key performance indicators such as cyclic working capacity, enthalpy of desorption, and CO_2 diffusion coefficients. These selection criteria were used due to their influence on the techno-economic feasibility of the CO_2 capture process. The inclusion of all selection criteria assisted in capturing the trade-offs between CO_2 solubility, energy of regeneration, and mass transfer. It was determined that the performance of the majority of ILs was far more superior to DESs at the examined conditions, mainly in terms of working capacity. The most promising solvent identified with the framework developed in this work was $[C_4 py][NTf_2]$ IL due to its high working capacity, low enthalpy of desorption, and high CO_2 diffusion coefficient. A comparison with selected physical solvent aqueous amines at the same conditions shows that even the best performer solvents investigated in this work present lower CO_2 loading capacity and higher solvent consumption, while

they show a clear advantage in terms of the enthalpy of desorption. Still for a fair detailed assessment, the best operating conditions for each solvent should be investigated separately.

Overall, this work demonstrates the promise held by SAFT-based models, specifically the soft-SAFT EoS, for the design of screening tools for solvents for CO_2 capture that assist in guiding the development and selection of the most promising systems, based on key process parameters. The procedure developed in this work has a high degree of reliability and robustness, being flexible to investigate the effects of a wide range of operating conditions on the performance of the examined solvents for CO_2 capture. An additional factor to be included in future work for a more holistic screening of solvents will be the inclusion of selectivity and the effect of impurities on the CO_2 capture performance of ILs and DESs. Also, please notice that the cost of the solvent, key in the case of ILs for large scale applications, was not considered in this work, as it was based on thermophysical properties.

As a final remark, results presented here are a showcase on how SAFT models and their application have evolved since the original publication 30 years ago, from some refined VLE calculations of complex fluids compared to simpler EoS, to the prediction of a whole set of required thermophysical properties for process design and its application to current environmental/engineering challenges.

■ ASSOCIATED CONTENT

ⓈI Supporting Information

The Supporting Information is available free of charge at https://pubs.acs.org/doi/10.1021/acs.jced.0c00750.

Soft-SAFT molecular parameters, FVT parameters of pure fluids, binary interaction parameters for CO_2 + ILs/DESs, and validation results for pure solvent liquid density (PDF)

■ AUTHOR INFORMATION

Corresponding Author

Lourdes F. Vega − *Research and Innovation Center on CO2 and H2 (RICH), Chemical Engineering Department, and Center for Catalysis and Separation (CeCaS), Khalifa University of Science and Technology, Abu Dhabi, United Arab Emirates;* ⓞ orcid.org/0000-0002-7609-4184; Email: lourdes.vega@ku.ac.ae

Authors

Ismail I. I. Alkhatib − *Research and Innovation Center on CO2 and H2 (RICH) and Chemical Engineering Department, Khalifa University of Science and Technology, Abu Dhabi, United Arab Emirates;* ⓞ orcid.org/0000-0002-6769-5383

Margarida L. Ferreira − *LAQV, REQUIMTE, Departamento de Química, Faculdade de Ciências e Tecnologia, Universidade Nova de Lisboa, 2829-516 Caparica, Portugal;* ⓞ orcid.org/0000-0002-8119-3881

Carlos G. Alba − *Research and Innovation Center on CO2 and H2 (RICH) and Chemical Engineering Department, Khalifa University of Science and Technology, Abu Dhabi, United Arab Emirates; Department of Chemical Engineering and Materials Science, IQS School of Engineering, Universitat Ramon Llull, 08017 Barcelona, Spain*

Daniel Bahamon − *Research and Innovation Center on CO2 and H2 (RICH), Chemical Engineering Department, and*

Center for Catalysis and Separation (CeCaS), Khalifa University of Science and Technology, Abu Dhabi, United Arab Emirates

Fèlix Llovell − Department of Chemical Engineering and Materials Science, IQS School of Engineering, Universitat Ramon Llull, 08017 Barcelona, Spain

Ana B. Pereiro − LAQV, REQUIMTE, Departamento de Química, Faculdade de Ciências e Tecnologia, Universidade Nova de Lisboa, 2829-516 Caparica, Portugal; orcid.org/0000-0001-7166-6764

João M. M. Araújo − LAQV, REQUIMTE, Departamento de Química, Faculdade de Ciências e Tecnologia, Universidade Nova de Lisboa, 2829-516 Caparica, Portugal; orcid.org/0000-0002-8648-7539

Mohammad R.M. Abu-Zahra − Research and Innovation Center on CO2 and H2 (RICH) and Chemical Engineering Department, Khalifa University of Science and Technology, Abu Dhabi, United Arab Emirates; orcid.org/0000-0001-8781-1727

Complete contact information is available at:
https://pubs.acs.org/10.1021/acs.jced.0c00750

Author Contributions

Ismail I. I. Alkhatib carried soft-SAFT calculations, data analyses and interpretation, and first writing of the manuscript. Margarida L. Ferreira and Carlos G. Alba performed calculations at different conditions and interpretation of them. Fèlix Lovell, Ana B. Pereiro, and João M. M. Araújo contributed to the design and interpretation of the calculations. Daniel Bahamon and Mohammad R. M. Abu-Zahra helped in the contextual analysis of the results and the figures. Lourdes F. Vega, together with Ismail I. I. Alkhatib, defined the strategy of the work, followed up on the results and interpretation and revised the overall work. All named authors have contributed to the drafting and the revision of the article.

Notes

The authors declare no competing financial interest.

REFERENCES

(1) British Petroleum (BP). Statistical Review of World Energy 2020 https://www.bp.com/en/global/corporate/energy-economics/statistical-review-of-world-energy.html (accessed 2020-07-09).

(2) IEA, I.E.A. Global CO2 emissions in 2019—Analysis https://www.iea.org/articles/global-co2-emissions-in-2019 (accessed 2020-07-19).

(3) Boot-Handford, M. E.; Abanades, J. C.; Anthony, E. J.; Blunt, M. J.; Brandani, S.; Mac Dowell, N.; Fernández, J. R.; Ferrari, M. C.; Gross, R.; Hallett, J. P.; Haszeldine, R. S.; Heptonstall, P.; Lyngfelt, A.; Makuch, Z.; Mangano, E.; Porter, R. T. J.; Pourkashanian, M.; Rochelle, G. T.; Shah, N.; Yao, J. G.; Fennell, P. S. Carbon Capture and Storage Update. Energy Environ. Sci. 2014, 7, 130−189.

(4) Mondal, M. K.; Balsora, H. K.; Varshney, P. Progress and Trends in CO2 Capture/Separation Technologies: A Review. Energy 2012, 46, 431−441.

(5) MacDowell, N.; Florin, N.; Buchard, A.; Hallett, J.; Galindo, A.; Jackson, G.; Adjiman, C. S.; Williams, C. K.; Shah, N.; Fennell, P. An Overview of CO2 Capture Technologies. Energy Environ. Sci. 2010, 11, 1645−1669.

(6) Mumford, K. A.; Wu, Y.; Smith, K. H.; Stevens, G. W. Review of Solvent Based Carbon-Dioxide Capture Technologies. Front. Chem. Sci. Eng. 2015, 9, 125−141.

(7) Aghaie, M.; Rezaei, N.; Zendehboudi, S. A Systematic Review on CO2 Capture with Ionic Liquids: Current Status and Future Prospects. Renewable Sustainable Energy Rev. 2018, 96, 502−525.

(8) Francisco, M.; Van Den Bruinhorst, A.; Kroon, M. C. Low-Transition-Temperature Mixtures (LTTMs): A New Generation of Designer Solvents. Angew. Chem., Int. Ed. 2013, 52, 3074−3085.

(9) Sarmad, S.; Mikkola, J.-P.; Ji, X. CO2 Capture with Ionic Liquids (ILs) and Deep Eutectic Solvents (DESs): A New Generation of Sorbents. ChemSusChem 2017, 10, 324−352.

(10) Vega, L. F.; Vilaseca, O.; Llovell, F.; Andreu, J. S. Modeling Ionic Liquids and the Solubility of Gases in Them: Recent Advances and Perspectives. Fluid Phase Equilib. 2010, 294, 15−30.

(11) Alkhatib, I. I. I.; Bahamon, D.; Llovell, F.; Abu-Zahra, M. R. M.; Vega, L. F. Perspectives and Guidelines on Thermodynamic Modelling of Deep Eutectic Solvents. J. Mol. Liq. 2020, 298, 112183.

(12) Shukla, S. K.; Khokarale, S. G.; Bui, T. Q.; Mikkola, J. P. T. Ionic Liquids: Potential Materials for Carbon Dioxide Capture and Utilization. Front. Mater. 2019, 6, 1−8.

(13) Theo, W. L.; Lim, J. S.; Hashim, H.; Mustaffa, A. A.; Ho, W. S. Review of Pre-Combustion Capture and Ionic Liquid in Carbon Capture and Storage. Appl. Energy 2016, 183, 1633−1663.

(14) Torralba-Calleja, E.; Skinner, J.; Gutiérrez-Tauste, D. CO 2 Capture in Ionic Liquids: A Review of Solubilities and Experimental Methods. J. Chem. 2013, 2013, 1−16.

(15) Zhang, X.; Zhang, X.; Dong, H.; Zhao, Z.; Zhang, S.; Huang, Y. Carbon Capture with Ionic Liquids: Overview and Progress. Energy Environ. Sci. 2012, 5, 6668−6681.

(16) Zhao, Z.; Dong, H.; Zhang, X. The Research Progress of CO2 Capture with Ionic Liquids. Chin. J. Chem. Eng. 2012, 20, 120−129.

(17) Aissaoui, T.; Alnashef, I. M.; Qureshi, U. A.; Benguerba, Y. Potential Applications of Deep Eutectic Solvents in Natural Gas Sweetening for CO2 Capture. Rev. Chem. Eng. 2017, 33, 523−550.

(18) Florindo, C.; Lima, F.; Ribeiro, B. D.; Marrucho, I. M. Deep Eutectic Solvents: Overcoming 21st Century Challenges. Curr. Opin. Green Sustain. Chem. 2019, 18, 31−36.

(19) Ge, X.; Gu, C.; Wang, X.; Tu, J. Deep Eutectic Solvents (DESs)-Derived Advanced Functional Materials for Energy and Environmental Applications: Challenges, Opportunities, and Future Vision. J. Mater. Chem. A 2017, 5, 8209−8229.

(20) Ma, C.; Sarmad, S.; Mikkola, J. P.; Ji, X. Development of Low-Cost Deep Eutectic Solvents for CO2 Capture. Energy Procedia 2017, 142, 3320−3325.

(21) Pereiro, A. B.; Araújo, J. M. M.; Esperança, J. M. S. S.; Marrucho, I. M.; Rebelo, L. P. N. Ionic Liquids in Separations of Azeotropic Systems - A Review. J. Chem. Thermodyn. 2012, 46, 2−28.

(22) Zhang, Y.; Ji, X.; Lu, X. Choline-Based Deep Eutectic Solvents for CO2 Separation: Review and Thermodynamic Analysis. Renewable Sustainable Energy Rev. 2018, 97, 436−455.

(23) Abu-Zahra, M. R. M.; Schneiders, L. H. J.; Niederer, J. P. M.; Feron, P. H. M.; Versteeg, G. F. CO2 Capture from Power Plants. Part I. A Parametric Study of the Technical Performance Based on Monoethanolamine. Int. J. Greenhouse Gas Control 2007, 1, 37−46.

(24) Abu-Zahra, M. R. M.; Niederer, J. P. M.; Feron, P. H. M.; Versteeg, G. F. CO2 Capture from Power Plants. Part II. A Parametric Study of the Economical Performance Based on Mono-Ethanolamine. Int. J. Greenhouse Gas Control 2007, 1, 135−142.

(25) Mota-Martinez, M. T.; Hallett, J.; MacDowell, N. Screening Solvents Properties for CO2 Capture Based on the Process Performance. Energy Procedia 2017, 114, 1551−1557.

(26) Tan, Y.; Nookuea, W.; Li, H.; Thorin, E.; Yan, J. Property Impacts on Carbon Capture and Storage (CCS) Processes: A Review. *Energy Convers. Manage.* **2016**, *118*, 204−222.

(27) Pereira, L. M. C.; Vega, L. F. A Systematic Approach for the Thermodynamic Modelling of CO2-Amine Absorption Process Using Molecular-Based Models. *Appl. Energy* **2018**, *232*, 273−291.

(28) Alkhatib, I. I. I.; Pereira, L. M. C.; Vega, L. F. 110th Anniversary: Accurate Modeling of the Simultaneous Absorption of H2S and CO2 in Aqueous Amine Solvents. *Ind. Eng. Chem. Res.* **2019**, *58*, 6870−6886.

(29) Alkhatib, I. I. I.; Pereira, L. M. C.; Alhajaj, A.; Vega, L. F. Performance of Non-Aqueous Amine Hybrid Solvents Mixtures for CO2 Capture: A Study Using a Molecular-Based Model. *J. CO2 Util.* **2020**, *35*, 126−144.

(30) Bahamon, D.; Alkhatib, I. I. I.; Alkhatib, N.; Builes, S.; Sinnokrot, M.; Vega, L. F. A Comparative Assessment of Emerging Solvents and Adsorbents for Mitigating CO2 Emissions from the Industrial Sector by Using Molecular Modeling Tools. *Front. Energy Res.* **2020**, *8*, 165.

(31) Bahamon, D.; Vega, L. F. Systematic Evaluation of Materials for Post-Combustion CO2 Capture in a Temperature Swing Adsorption Process. *Chem. Eng. J.* **2016**, *284*, 438−447.

(32) Bahamon, D.; Díaz-Márquez, A.; Gamallo, P.; Vega, L. F. Energetic Evaluation of Swing Adsorption Processes for CO2 Capture in Selected MOFs and Zeolites: Effect of Impurities. *Chem. Eng. J.* **2018**, *342*, 458−473.

(33) Xie, Y.; Liu, G.; Nie, H.; Yu, F.; Xing, X.; Cui, H. Energy Analysis of Physical Absorption and Chemical Absorption of CO2 in Ionic Liquids. *Energy Technol.* **2020**, *8*, 1−7.

(34) Venkatraman, V.; Evjen, S.; Lethesh, K. C.; Raj, J. J.; Knuutila, H. K.; Fiksdahl, A. Rapid, Comprehensive Screening of Ionic Liquids towards Sustainable Applications. *Sustain. Energy Fuels* **2019**, *3*, 2798−2808.

(35) Ali, E.; Hadj-Kali, M. K.; Alnashef, I. Modeling of CO2 Solubility in Selected Imidazolium-Based Ionic Liquids. *Chem. Eng. Commun.* **2017**, *204*, 205−215.

(36) Wang, J.; Song, Z.; Cheng, H.; Chen, L.; Deng, L.; Qi, Z. Computer-Aided Design of Ionic Liquids as Absorbent for Gas Separation Exemplified by CO2 Capture Cases. *ACS Sustainable Chem. Eng.* **2018**, *6*, 12025−12035.

(37) Hadj-Kali, M. K.; Althuluth, M.; Mokraoui, S.; Wazeer, I.; Ali, E.; Richon, D. Screening of Ionic Liquids for Gas Separation Using COSMO-RS and Comparison between Performances of Ionic Liquids and Aqueous Alkanolamine Solutions. *Chem. Eng. Commun.* **2020**, *207*, 1−14.

(38) Palomar, J.; Gonzalez-Miquel, M.; Polo, A.; Rodriguez, F. Understanding the Physical Absorption of CO2 in Ionic Liquids Using the COSMO-RS Method. *Ind. Eng. Chem. Res.* **2011**, *50*, 3452−3463.

(39) Sumon, K. Z.; Henni, A. Ionic Liquids for CO2 Capture Using COSMO-RS: Effect of Structure, Properties and Molecular Interactions on Solubility and Selectivity. *Fluid Phase Equilib.* **2011**, *310*, 39−55.

(40) de Riva, J.; Suarez-Reyes, J.; Moreno, D.; Díaz, I.; Ferro, V.; Palomar, J. Ionic Liquids for Post-Combustion CO2 Capture by Physical Absorption: Thermodynamic, Kinetic and Process Analysis. *Int. J. Greenhouse Gas Control* **2017**, *61*, 61−70.

(41) Maiti, A. Theoretical Screening of Ionic Liquid Solvents for Carbon Capture. *ChemSusChem* **2009**, *2*, 628−631.

(42) Liu, Y.; Yu, H.; Sun, Y.; Zeng, S.; Zhang, X.; Nie, Y.; Zhang, S.; Ji, X. Screening Deep Eutectic Solvents for CO2 Capture With COSMO-RS. *Front. Chem.* **2020**, *8*, 1−11.

(43) Venkatraman, V.; Alsberg, B. K. Predicting CO2 Capture of Ionic Liquids Using Machine Learning. *J. CO2 Util.* **2017**, *21*, 162−168.

(44) Xie, Y.; Zhang, Y.; Lu, X.; Ji, X. Energy Consumption Analysis for CO2 Separation Using Imidazolium-Based Ionic Liquids. *Appl. Energy* **2014**, *136*, 325−335.

(45) Liu, X.; Huang, Y.; Zhao, Y.; Gani, R.; Zhang, X.; Zhang, S. Ionic Liquid Design and Process Simulation for Decarbonization of Shale Gas. *Ind. Eng. Chem. Res.* **2016**, *55*, 5931−5944.

(46) Mota-Martinez, M. T.; Brandl, P.; Hallett, J. P.; Mac Dowell, N. Challenges and Opportunities for the Utilisation of Ionic Liquids as Solvents for CO2 Capture. *Mol. Syst. Des. Eng.* **2018**, *3*, 560−571.

(47) Basha, O. M. *Process Based Screening Method and Systems Analysis for Pre-Combustion Carbon Capture Using Ionic Liquids*; Elsevier Masson SAS, 2019; Vol. 47.

(48) Zhang, Y.; Ji, X.; Xie, Y.; Lu, X. Thermodynamic Analysis of CO2 Separation from Biogas with Conventional Ionic Liquids. *Appl. Energy* **2018**, *217*, 75−87.

(49) Zhang, Y.; Ji, X.; Xie, Y.; Lu, X. Screening of Conventional Ionic Liquids for Carbon Dioxide Capture and Separation. *Appl. Energy* **2016**, *162*, 1160−1170.

(50) Haider, M. B.; Jha, D.; Marriyappan Sivagnanam, B.; Kumar, R. Modelling and Simulation of CO2 Removal from Shale Gas Using Deep Eutectic Solvents. *J. Environ. Chem. Eng.* **2019**, *7*, 102747.

(51) Ma, C.; Xie, Y.; Ji, X.; Liu, C.; Lu, X. Modeling, Simulation and Evaluation of Biogas Upgrading Using Aqueous Choline Chloride/Urea. *Appl. Energy* **2018**, *229*, 1269−1283.

(52) Baghban, A.; Ahmadi, M. A.; Shahraki, B. H. Prediction Carbon Dioxide Solubility in Presence of Various Ionic Liquids Using Computational Intelligence Approaches. *J. Supercrit. Fluids* **2015**, *98*, 50−64.

(53) Paduszyński, K.; Domańska, U. Viscosity of Ionic Liquids: An Extensive Database and a New Group Contribution Model Based on a Feed-Forward Artificial Neural Network. *J. Chem. Inf. Model.* **2014**, *54*, 1311−1324.

(54) Zhang, X.; Liu, Z.; Wang, W. Screening of Ionic Liquids to Capture CO2 by COSMO-RS and Experiments. *AIChE J.* **2008**, *54*, 2717−2728.

(55) Zhao, Y.; Huang, Y.; Zhang, X.; Zhang, S. A Quantitative Prediction of the Viscosity of Ionic Liquids Using $S\sigma$-Profile Molecular Descriptors. *Phys. Chem. Chem. Phys.* **2015**, *17*, 3761−3767.

(56) Chapman, W. G.; Gubbins, K. E.; Jackson, G.; Radosz, M. SAFT: Equation-of-State Solution Model for Associating Fluids. *Fluid Phase Equilib.* **1989**, *52*, 31−38.

(57) Chapman, W. G.; Gubbins, K. E.; Jackson, G.; Radosz, M. New Reference Equation of State for Associating Liquids. *Ind. Eng. Chem. Res.* **1990**, *29*, 1709−1721.

(58) Huang, S. H.; Radosz, M. Equation of State for Small, Large, Polydisperse, and Associating Molecules. *Ind. Eng. Chem. Res.* **1990**, *29*, 2284−2294.

(59) Huang, S. H.; Radosz, M. Equation of State for Small, Large, Polydisperse, and Associating Molecules: Extension to Fluid Mixtures. *Ind. Eng. Chem. Res.* **1991**, *30*, 1994−2005.

(60) Wertheim, M. S. Fluids with Highly Directional Attractive Forces. I. Statistical Thermodynamics. *J. Stat. Phys.* **1984**, *35*, 19−34.

(61) Wertheim, M. S. Fluids with Highly Directional Attractive Forces. II. Thermodynamic Perturbation Theory and Integral Equations. *J. Stat. Phys.* **1984**, *35*, 35−47.

(62) Wertheim, M. S. Fluids with Highly Directional Attractive Forces. III. Multiple Attraction Sites. *J. Stat. Phys.* **1986**, *42*, 459−476.

(63) Wertheim, M. S. Fluids with Highly Directional Attractive Forces. IV. Equilibrium Polymerization. *J. Stat. Phys.* **1986**, *42*, 477−492.

(64) Vega, L. F.; Llovell, F. Review and New Insights into the Application of Molecular-Based Equations of State to Water and Aqueous Solutions. *Fluid Phase Equilib.* **2016**, *416*, 150−173.

(65) Blas, F. J.; Vega, L. F. Thermodynamic Behaviour of Homonuclear and Heteronuclear Lennard-Jones Chains with Association Sites from Simulation and Theory. *Mol. Phys.* **1997**, *92*, 135−150.

(66) Blas, F. J.; Vega, L. F. Prediction of Binary and Ternary Diagrams Using the Statistical Associating Fluid Theory (SAFT) Equation of State. *Ind. Eng. Chem. Res.* **1998**, *37*, 660−674.

(67) Asensio-Delgado, S.; Jovell, D.; Zarca, G.; Urtiaga, A.; Llovell, F. Thermodynamic and Process Modeling of the Recovery of R410A Compounds with Ionic Liquids. *Int. J. Refrig.* **2020**, *118*, 365−375.

(68) Andreu, J. S.; Vega, L. F. Capturing the Solubility Behavior of CO2 in Ionic Liquids by a Simple Model. *J. Phys. Chem. C* **2007**, *111*, 16028−16034.

(69) Llovell, F.; Valente, E.; Vilaseca, O.; Vega, L. F. Modeling Complex Associating Mixtures with [Cn-Mim][Tf2N] Ionic Liquids: Predictions from the Soft-SAFT Equation. *J. Phys. Chem. B* **2011**, *115*, 4387−4398.

(70) Pereira, L. M. C.; Oliveira, M. B.; Dias, A. M. A.; Llovell, F.; Vega, L. F.; Carvalho, P. J.; Coutinho, J. A. P. High Pressure Separation of Greenhouse Gases from Air with 1-Ethyl-3-Methyl-imidazolium Methyl-Phosphonate. *Int. J. Greenhouse Gas Control* **2013**, *19*, 299−309.

(71) Llovell, F.; Oliveira, M. B.; Coutinho, J. A. P.; Vega, L. F. Solubility of Greenhouse and Acid Gases on the [C4mim][MeSO4] Ionic Liquid for Gas Separation and CO2 conversion. *Catal. Today* **2015**, *255*, 87−96.

(72) Pereiro, A. B.; Llovell, F.; Araújo, J. M. M.; Santos, A. S. S.; Rebelo, L. P. N.; Piñeiro, M. M.; Vega, L. F. Thermophysical Characterization of Ionic Liquids Based on the Perfluorobutanesulfonate Anion: Experimental and Soft-SAFT Modeling Results. *ChemPhysChem* **2017**, *18*, 2012−2023.

(73) Ferreira, M. L.; Llovell, F.; Vega, L. F.; Pereiro, A. B.; Araújo, J. M. M. Systematic Study of the Influence of the Molecular Structure of Fluorinated Ionic Liquids on the Solubilization of Atmospheric Gases Using a Soft-SAFT Based Approach. *J. Mol. Liq.* **2019**, *294*, 111645.

(74) Alonso, G.; Gamallo, P.; Sayós, R.; Llovell, F. Combining Soft-SAFT and COSMO-RS Modeling Tools to Assess the CO2−SO2 Separation Using Phosphonium-Based Ionic Liquids. *J. Mol. Liq.* **2020**, *297*, 111795.

(75) Albà, C. G.; Vega, L. F.; Llovell, F. Assessment on Separating Hydrofluoroolefins from Hydrofluorocarbons at the Azeotropic Mixture R513A by Using Fluorinated Ionic Liquids: A Soft-SAFT Study. *Ind. Eng. Chem. Res.* **2020**, *59*, 13315−13324.

(76) Lloret, J. O.; Vega, L. F.; Llovell, F. Accurate Description of Thermophysical Properties of Tetraalkylammonium Chloride Deep Eutectic Solvents with the Soft-SAFT Equation of State. *Fluid Phase Equilib.* **2017**, *448*, 81−93.

(77) Ojeda, R. M.; Llovell, F. Soft-SAFT Transferable Molecular Models for the Description of Gas Solubility in Eutectic Ammonium Salt-Based Solvents. *J. Chem. Eng. Data* **2018**, *63*, 2599−2612.

(78) Crespo, E. A.; Silva, L.; Lloret, J. O.; Carvalho, P. J.; Vega, L. F.; Llovell, F.; Coutinho, J. A. P. A Methodology to Parameterize SAFT-Type Equations of State for Solid Precursors of Deep Eutectic Solvents: The Example of Cholinium Chloride. *Phys. Chem. Chem. Phys.* **2019**, *2*, 15046−15061.

(79) Johnson, J. K.; Zollweg, J. A.; Gubbins, K. E. The Lennard-Jones Equation of State Revisited. *Mol. Phys.* **1993**, *78*, 591−618.

(80) Gubbins, K. E.; Twu, C. H. Thermodynamics of Polyatomic Fluid Mixtures-I: Theory. *Chem. Eng. Sci.* **1978**, *33*, 863−878.

(81) Twu, C. H.; Gubbins, K. E. Thermodynamics of Polyatomic Fluid Mixtures—II: Polar, Quadrupolar and Octopolar Molecules. *Chem. Eng. Sci.* **1978**, *33*, 879−887.

(82) Jog, P. K.; Chapman, W. G. Application of Wertheim's Thermodynamic Perturbation Theory to Dipolar Hard Sphere Chains. *Mol. Phys.* **1999**, *97*, 307−319.

(83) Jog, P. K.; Sauer, S. G.; Blaesing, J.; Chapman, W. G. Application of Dipolar Chain Theory to the Phase Behavior of Polar Fluids and Mixtures. *Ind. Eng. Chem. Res.* **2001**, *40*, 4641−4648.

(84) Alkhatib, I. I. I.; Pereira, L. M. C.; Torne, J.; Vega, L. F. Polar Soft-SAFT: Theory and Comparison with Molecular Simulations and Experimental Data of Pure Polar Fluids. *Phys. Chem. Chem. Phys.* **2020**, *22*, 13171−13191.

(85) Alkhatib, I. I. I.; Vega, L. F. Quantifying the Effect of Polarity on the Behavior of Mixtures of n-Alkanes with Dipolar Solvents Using Polar Soft-SAFT. *AIChE J.* **2020**, No. e16649.

(86) Allal, A.; Boned, C.; Baylaucq, A. Free-Volume Viscosity Model for Fluids in the Dense and Gaseous States. *Phys. Rev. E: Stat. Phys., Plasmas, Fluids, Relat. Interdiscip. Top.* **2001**, *64*, 011203.

(87) Allal, A.; Moha-Ouchane, M.; Boned, C. A New Free-Volume Model for Dynamic Viscosity and Density of Dense Fluids Versus Pressure and Temperature. *Phys. Chem. Liq.* **2006**, *39*, 1−30.

(88) Pereira, L. M. C.; Llovell, F.; Vega, L. F. Thermodynamic Characterisation of Aqueous Alkanolamine and Amine Solutions for Acid Gas Processing by Transferable Molecular Models. *Appl. Energy* **2018**, *222*, 687−703.

(89) Llovell, F.; Marcos, R. M.; Vega, L. F. Free-Volume-Theory Coupled with Soft-SAFT for Viscosity Calculations: Comparison with Molecular Simulation and Experimental Data. *J. Phys. Chem. B* **2013**, *117*, 8159−8171.

(90) Llovell, F.; Marcos, R. M.; Vega, L. F. Transport Properties of Mixtures by the Soft-SAFT + Free-Volume Theory: Application to Mixtures of n-Alkanes and Hydrofluorocarbons. *J. Phys. Chem. B* **2013**, *117*, 5195−5205.

(91) Moganty, S. S.; Baltus, R. E. Diffusivity of Carbon Dioxide in Room-Temperature Ionic Liquids. *Ind. Eng. Chem. Res.* **2010**, *49*, 9370−9376.

(92) Moya, C.; Palomar, J.; Gonzalez-Miquel, M.; Bedia, J.; Rodriguez, F. Diffusion Coefficients of CO2 in Ionic Liquids Estimated by Gravimetry. *Ind. Eng. Chem. Res.* **2014**, *53*, 13782−13789.

(93) Wilke, C. R.; Chang, P. Correlation of Diffusion Coefficients in Dilute Solutions. *AIChE J.* **1955**, *1*, 264−270.

(94) Xie, Y.; Ma, C.; Lu, X.; Ji, X. Evaluation of Imidazolium-Based Ionic Liquids for Biogas Upgrading. *Appl. Energy* **2016**, *175*, 69−81.

(95) Zhai, H.; Rubin, E. S. Systems Analysis of Physical Absorption of CO2 in Ionic Liquids for Pre-Combustion Carbon Capture. *Environ. Sci. Technol.* **2018**, *52*, 4996−5004.

(96) Pedrosa, N.; Pámies, J. C.; Coutinho, J. A. P.; Marrucho, I. M.; Vega, L. F. Phase Equilibria of Ethylene Glycol Oligomers and Their Mixtures. *Ind. Eng. Chem. Res.* **2005**, *44*, 7027−7037.

(97) Dias, A. M. A.; Carrier, H.; Daridon, J. L.; Pàmies, J. C.; Vega, L. F.; Coutinho, J. A. P.; Marrucho, I. M. Vapor - Liquid Equilibrium of Carbon Dioxide - Perfluoroalkane Mixtures: Experimental Data and SAFT Modeling. *Ind. Eng. Chem. Res.* **2006**, *45*, 2341−2350.

(98) Llovell, F. *Advanced Models: Association Theories and Models*; Elsevier Inc., 2018.

(99) Mac Dowell, N.; Llovell, F.; Sun, N.; Hallet, J. P.; George, A.; Hunt, P. A.; Welton, T.; Simmons, B. A.; Vega, L. F. New Experimental Density Data and Soft-SAFT Models of Alkylimidazolium ([CnC1im]+) Chloride (Cl-), Methylsulfate ([MeSO4]-), and Dimethylphosphate ([Me2PO4]-) Based Ionic Liquids. *J. Phys. Chem. B* **2014**, *118*, 6206−6221.

(100) Zarca, G.; Ortiz, I.; Urtiaga, A.; Llovell, F. Accurate Thermodynamic Modeling of Ionic Liquids/Metal Salt Mixtures: Application to Carbon Monoxide Reactive Absorption. *AIChE J.* **2017**, *63*, 3532−3543.

(101) Pereira, L. M. C.; Oliveira, M. B.; Llovell, F.; Vega, L. F.; Coutinho, J. A. P. Assessing the N2O/CO2 High Pressure Separation Using Ionic Liquids with the Soft-SAFT EoS. *J. Supercrit. Fluids* **2014**, *92*, 231−241.

(102) Ferreira, M. L.; Araújo, J. M. M.; Pereiro, A. B.; Vega, L. F. Insights into the Influence of the Molecular Structures of Fluorinated Ionic Liquids on Their Thermophysical Properties. A Soft-SAFT Based Approach. *Phys. Chem. Chem. Phys.* **2019**, *21*, 6362−6380.

(103) Jacquemin, J.; Husson, P.; Padua, A. A. H.; Majer, V. Density and Viscosity of Several Pure and Water-Saturated Ionic Liquids. *Green Chem.* **2006**, *8*, 172−180.

(104) Tariq, M.; Serro, A. P.; Mata, J. L.; Saramago, B.; Esperança, J. M. S. S.; Lopes, J. N. C.; Rebelo, L. P. N. High-Temperature Surface Tension and Density Measurements of 1-Alkyl-3-Methylimidazolium Bistriflamide Ionic Liquids. *Fluid Phase Equilib.* **2010**, *294*, 131−138.

(105) Vakili-Nezhaad, G.; Vatani, M.; Asghari, M.; Ashour, I. Effect of Temperature on the Physical Properties of 1-Butyl-3- Methyl-imidazolium Based Ionic Liquids with Thiocyanate and Tetrafluor-

oborate Anions, and 1-Hexyl-3-Methylimidazolium with Tetrafluoroborate and Hexafluorophosphate Anions. *J. Chem. Thermodyn.* **2012**, *54*, 148−154.

(106) Vieira, N. S. M.; Reis, P. M.; Shimizu, K.; Cortes, O. A.; Marrucho, I. M.; Araújo, J. M. M.; Esperança, J. M. S. S.; Lopes, J. N. C.; Pereiro, A. B.; Rebelo, L. P. N. A Thermophysical and Structural Characterization of Ionic Liquids with Alkyl and Perfluoroalkyl Side Chains. *RSC Adv.* **2015**, *5*, 65337−65350.

(107) Watanabe, M.; Kodama, D.; Makino, T.; Kanakubo, M. CO_2 Absorption Properties of Imidazolium Based Ionic Liquids Using a Magnetic Suspension Balance. *Fluid Phase Equilib.* **2016**, *420*, 44−49.

(108) Yadav, A.; Trivedi, S.; Rai, R.; Pandey, S. Densities and Dynamic Viscosities of (Choline Chloride+glycerol) Deep Eutectic Solvent and Its Aqueous Mixtures in the Temperature Range (283.15−363.15)K. *Fluid Phase Equilib.* **2014**, *367*, 135−142.

(109) Li, G.; Jiang, Y.; Liu, X.; Deng, D. New Levulinic Acid-Based Deep Eutectic Solvents: Synthesis and Physicochemical Property Determination. *J. Mol. Liq.* **2016**, *222*, 201−207.

(110) Leron, R. B.; Li, M. H. High-Pressure Volumetric Properties of Choline Chloride-Ethylene Glycol Based Deep Eutectic Solvent and Its Mixtures with Water. *Thermochim. Acta* **2012**, *546*, 54−60.

(111) Zubeir, L. F.; Held, C.; Sadowski, G.; Kroon, M. C. PC-SAFT Modeling of CO_2 Solubilities in Deep Eutectic Solvents. *J. Phys. Chem. B* **2016**, *120*, 2300−2310.

(112) Cané, E.; Llovell, F.; Vega, L. F. Accurate Viscosity Predictions of Linear Polymers from N-Alkanes Data. *J. Mol. Liq.* **2017**, *243*, 115−123.

(113) Zubeir, L. F.; Lacroix, M. H. M.; Kroon, M. C. Low Transition Temperature Mixtures as Innovative and Sustainable CO_2 Capture Solvents. *J. Phys. Chem. B* **2014**, *118*, 14429−14441.

(114) Yusof, R.; Abdulmalek, E.; Sirat, K.; Rahman, M. B. A. Tetrabutylammonium Bromide (TBABr)-Based Deep Eutectic Solvents (DESs) and Their Physical Properties. *Molecules* **2014**, *19*, 8011−8026.

(115) Mjalli, F. S.; Naser, J.; Jibril, B.; Alizadeh, V.; Gano, Z. Tetrabutylammonium Chloride Based Ionic Liquid Analogues and Their Physical Properties. *J. Chem. Eng. Data* **2014**, *59*, 2242−2251.

(116) Harifi-Mood, A. R.; Buchner, R. Density, Viscosity, and Conductivity of Choline Chloride + Ethylene Glycol as a Deep Eutectic Solvent and Its Binary Mixtures with Dimethyl Sulfoxide. *J. Mol. Liq.* **2017**, *225*, 689−695.

(117) Ge, M.; Ma, J.; Chu, B. Densities and Viscosities of Propane-1,2,3-Triol + Ethane-1,2-Diol at T) (298.15 to 338.15) K. *J. Chem. Eng. Data* **2010**, *55*, 2649−2651.

(118) Chemat, F.; You, H. J.; Muthukumar, K.; Murugesan, T. Effect of L-Arginine on the Physical Properties of Choline Chloride and Glycerol Based Deep Eutectic Solvents. *J. Mol. Liq.* **2015**, *212*, 605−611.

(119) Al-Dawsari, J. N.; Bessadok-Jemai, A.; Wazeer, I.; Mokraoui, S.; AlMansour, M. A.; Hadj-Kali, M. K. Fitting of Experimental Viscosity to Temperature Data for Deep Eutectic Solvents. *J. Mol. Liq.* **2020**, *310*, 113127.

(120) Rodríguez, H.; Brennecke, J. F. Temperature and Composition Dependence of the Density and Viscosity of Binary Mixtures of Water + Ionic Liquid. *J. Chem. Eng. Data* **2006**, *51*, 2145−2155.

(121) Almeida, H. F. D.; Canongia Lopes, J. N.; Rebelo, L. P. N.; Coutinho, J. A. P.; Freire, M. G.; Marrucho, I. M. Densities and Viscosities of Mixtures of Two Ionic Liquids Containing a Common Cation. *J. Chem. Eng. Data* **2016**, *61*, 2828−2843.

(122) Zeng, S.; Wang, J.; Bai, L.; Wang, B.; Gao, H.; Shang, D.; Zhang, X.; Zhang, S. Highly Selective Capture of CO2 by Ether-Functionalized Pyridinium Ionic Liquids with Low Viscosity. *Energy Fuels* **2015**, *29*, 6039−6048.

(123) Pereiro, A. B.; Verdía, P.; Tojo, E.; Rodríguez, A. Physical Properties of 1-Butyl-3-Methylimidazolium Methyl Sulfate as a Function of Temperature. *J. Chem. Eng. Data* **2007**, *52*, 377−380.

(124) Oliveira, F. S.; Freire, M. G.; Carvalho, P. J.; Coutinho, J. A. P.; Lopes, J. N. C.; Rebelo, L. P. N.; Marrucho, I. M. Structural and

(125) Neves, C. M. S. S.; Kurnia, K. A.; Coutinho, J. A. P.; Marrucho, I. M.; Lopes, J. N. C.; Freire, M. G.; Rebelo, L. P. N. Systematic Study of the Thermophysical Properties of Imidazolium-Based Ionic Liquids with Cyano-Functionalized Anions. *J. Phys. Chem. B* **2013**, *117*, 10271−10283.

(126) Liu, Q. S.; Li, P. P.; Welz-Biermann, U.; Chen, J.; Liu, X. X. Density, Dynamic Viscosity, and Electrical Conductivity of Pyridinium-Based Hydrophobic Ionic Liquids. *J. Chem. Thermodyn.* **2013**, *66*, 88−94.

(127) Iguchi, M.; Hiraga, Y.; Sato, Y.; Aida, T. M.; Watanabe, M.; Smith, R. L. Measurement of High-Pressure Densities and Atmospheric Viscosities of Ionic Liquids: 1-Hexyl-3-Methylimidazolium Bis(Trifluoromethylsulfonyl)Imide and 1-Hexyl-3-Methylimidazolium Chloride. *J. Chem. Eng. Data* **2014**, *59*, 709−717.

(128) Freire, M. G.; Teles, A. R. R.; Rocha, M. A. A.; Schröder, B.; Neves, C. M. S. S.; Carvalho, P. J.; Evtuguin, D. V.; Santos, L. M. N. B. F.; Coutinho, J. A. P. Thermophysical Characterization of Ionic Liquids Able to Dissolve Biomass. *J. Chem. Eng. Data* **2011**, *56*, 4813−4822.

(129) Das, S. K.; Sarkar, M. Probing Solute-Solvent Interaction in 1-Ethyl-3-Methylimidazolium-Based Room Temperature Ionic Liquids: A Time-Resolved Fluorescence Anisotropy Study. *J. Fluoresc.* **2014**, *24*, 455−463.

(130) Atilhan, M.; Jacquemin, J.; Rooney, D.; Khraisheh, M.; Aparicio, S. Viscous Behavior of Imidazolium-Based Ionic Liquids. *Ind. Eng. Chem. Res.* **2013**, *52*, 16774−16785.

(131) Zhou, L.; Fan, J.; Shang, X. CO_2 Capture and Separation Properties in the Ionic Liquid 1-n-Butyl-3-Methylimidazolium Nonafluorobutylsulfonate. *Materials* **2014**, *7*, 3867−3880.

(132) Zubeir, L. F.; Spyriouni, T.; Roest, D.; Hill, J. R.; Kroon, M. C. Effect of Oxygenation on Carbon Dioxide Absorption and Thermophysical Properties of Ionic Liquids: Experiments and Modeling Using Electrolyte PC-SAFT. *Ind. Eng. Chem. Res.* **2016**, *55*, 8869−8882.

(133) Yokozeki, A.; Shiflett, M. B.; Junk, C. P.; Grieco, L. M.; Foo, T. Physical and Chemical Absorptions of Carbon Dioxide in Room-Temperature Ionic Liquids. *J. Phys. Chem. B* **2008**, *112*, 16654−16663.

(134) Wang, X.; Zeng, S.; Wang, J.; Shang, D.; Zhang, X.; Liu, J.; Zhang, Y. Selective Separation of Hydrogen Sulfide with Pyridinium-Based Ionic Liquids. *Ind. Eng. Chem. Res.* **2018**, *57*, 1284−1293.

(135) Soriano, A. N.; Doma, B. T.; Li, M. H. Carbon Dioxide Solubility in 1-Ethyl-3-Methylimidazolium Trifluoromethanesulfonate. *J. Chem. Thermodyn.* **2009**, *41*, 525−529.

(136) Shiflett, M. B.; Niehaus, A. M. S.; Elliott, B. A.; Yokozeki, A. Phase Behavior of N_2O and CO_2 in Room-Temperature Ionic Liquids [Bmim][Tf_2N], [Bmim][BF_4], [Bmim][N(CN)$_2$], [Bmim][Ac], [Eam][NO_3], and [Bmim][SCN]. *Int. J. Thermophys.* **2012**, *33*, 412−436.

(137) Muldoon, M. J.; Aki, S. N. V. K.; Anderson, J. L.; Dixon, J. K.; Brennecke, J. F. Improving Carbon Dioxide Solubility in Ionic Liquids. *J. Phys. Chem. B* **2007**, *111*, 9001−9009.

(138) Moya, C.; Gonzalez-Miquel, M.; Rodriguez, F.; Soto, A.; Rodriguez, H.; Palomar, J. Non-Ideal Behavior of Ionic Liquid Mixtures to Enhance CO_2 Capture. *Fluid Phase Equilib.* **2017**, *450*, 175−183.

(139) Moganty, S. S.; Close, J.; Baltus, R. Solubilities and Diffusivities of Carbon Dioxide in Ionic Liquids. *AIChE Annu. Meet. Conf. Proc.* **2008**, 4453−4464.

(140) Makino, T.; Kanakubo, M.; Masuda, Y.; Umecky, T.; Suzuki, A. CO_2 Absorption Properties, Densities, Viscosities, and Electrical Conductivities of Ethylimidazolium and 1-Ethyl-3-Methylimidazolium Ionic Liquids. *Fluid Phase Equilib.* **2014**, *362*, 300−306.

(141) Leron, R. B.; Li, M. H. Solubility of Carbon Dioxide in a Eutectic Mixture of Choline Chloride and Glycerol at Moderate Pressures. *J. Chem. Thermodyn.* **2013**, *57*, 131−136.

(124) Oliveira, F. S.; Freire, M. G.; Carvalho, P. J.; Coutinho, J. A. P.; Lopes, J. N. C.; Rebelo, L. P. N.; Marrucho, I. M. Structural and Positional Isomerism Influence in the Physical Properties of Pyridinium NTf2-Based Ionic Liquids: Pure and Water-Saturated Mixtures. *J. Chem. Eng. Data* **2010**, *55*, 4514−4520.

(142) Leron, R. B.; Caparanga, A.; Li, M. H. Carbon Dioxide Solubility in a Deep Eutectic Solvent Based on Choline Chloride and Urea at T = 303.15−343.15K and Moderate Pressures. *J. Taiwan Inst. Chem. Eng.* **2013**, *44*, 879−885.

(143) Deng, D.; Jiang, Y.; Liu, X.; Zhang, Z.; Ai, N. Investigation of Solubilities of Carbon Dioxide in Five Levulinic Acid-Based Deep Eutectic Solvents and Their Thermodynamic Properties. *J. Chem. Thermodyn.* **2016**, *103*, 212−217.

(144) El Hadri, N.; Quang, D. V.; Goetheer, E. L. V.; Abu Zahra, M. R. M. Aqueous Amine Solution Characterization for Post-Combustion CO_2 Capture Process. *Appl. Energy* **2017**, *185*, 1433−1449.